UNIVERSITA' DEGLI STUDI DI PARMA

Dottorato di ricerca in Scienza e Tecnologia dei Materiali

Ciclo XXIX

Electronic synapses: bioinspired and biomimicking networks based on organic memristors.

Coordinatore:

Chia.mo Prof. Dalcanale

Tutor:

Dr. Salvatore Iannotta

Co-Tutor:

Dr. Victor Erokhin

Dottoranda:

Silvia Battistoni

A mio papà
per avermi ricordato a modo suo
che bella e preziosa famiglia che ho.

CONTENTS

LIST OF FIGURES

ABSTRACT

This thesis reports part of the results obtained during these 3 years of PhD program in which I have been involved in the MaDEleNA Project (Developing and Studying novel intelligent nanoMaterials and Devices towards Adaptive Electronics and Neuroscience Applications) founded by Provincia Autonoma di Trento. My research activity, based on the electrical properties of a special electrochemical device with memory features named Organic Memristor, embraces two of the most challenging fields of research: the neuromorphic engineering and the bio-electronics. We reported the realization of memristive devices able to perform typical features of the biological synaptic plasticity considering both the well studied Long Term Potentiation (LTP) and the Long Term Depression (LTD) homosynaptic functions and the less investigated heterosynaptic plasticity. Moreover, we realized artificial neuronal networks in which the main role was played by memristive devices whose ability of varying their conductive properties made possible the accomplishment of an elementary perceptron and, afterwards, of an artificial neuronal network that can be considered as a precursor of the double layer perceptron. Finally, we provided evidences of the possibility of interfacing of the organic memristor with different cells testing the bio-compatibility of the polymeric main component of the devices, and reporting proves of the possibility of connecting two nervous cells through an organic memristor preserving their biological communication mechanisms.

1 INTRODUCTION

Contents

1.1 MEMRISTOR: THE THEORY

Back in 1960, Widrow proposed the realization of a variable resistor fabricated using metal particles deposited on a pencil lead by means of the phenomenon of the electroplating [1] and even if such device was named memistor and had three terminals, necessary for the control of the deposition and the final properties' sensing, at the time, it was not linked to the fundamentals of circuit theory. 8 years later, Fano et al. in the book "Electromagnetic Fields, Energy, and Forces" described the existence of four fundamental circuital elements: resistor,

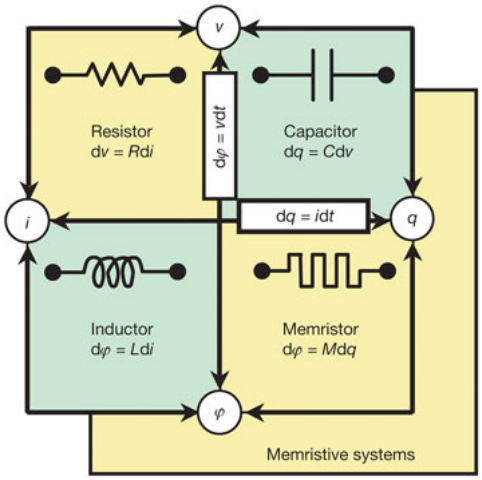

Figure 1.1: *Alternative representation of the relationships between the four fundamental circuit variables [4]*

capacitor, inductor, and an unknown element [2] that finally in 1971 Prof. Chua [3] in his famous paper "Memristor-The missing circuit element" described as a missing electronic element capable of varying its resistance depending on the amount of charge passed through it and provided the theoretical prove of its theory. The term memristor was originated by the contraction of *memory* and *resistor*, since such kind of element represents a hypothetical passive element whose resistance can vary, according to the history of the device.

The idea of his work turned around the symmetry of all properties and parameters in nature. Let us consider the four fundamental circuit variables: the current i, the voltage v, the charge q and the flux-linkage φ, that can be connected by the following relationships (Equ.1.1):

$$dq(t) = idt; \quad d\varphi = vdt; \quad dv = Rdi; \quad dq = Cdv; \quad d\varphi = Ldi \tag{1.1}$$

where the axiomatic definition of the resistor (R), the capacitor (C) and the inductor (L) are also included .

A more reader-friendly representation of the interconnections between the four fundamental circuit variables is the scheme reported above (Figure 1.1)

where only two variables remained unpaired: the charge and the flux linkage. Before the paper of Prof. Chua, in fact, it was impossible to connect them by a mathematical or a physical law, thus he postulated the existence of a missing circuit element the relationship of which can be written in Equ. 1.2 :

$$d\varphi = M(q)dq \tag{1.2}$$

that connects the charge and the flux linkage through the *Memristance* (M)[3]. Dimensionally, M is a resistance and its deep meaning can be easily understood starting from the equation, postulated by Chua in the same paper, of the tension across a memristor (Equ. 1.3) :

$$v(t) = M(q(t))i(t) \tag{1.3}$$

M, in fact, is also a function of the charge q, that by definition, depends over the current by a time integral (Equ.1.4):

$$v(t) = M(q)i(t) = M\left(\int i(t')dt'\right) i(t). \tag{1.4}$$

In other words, a memristor is resistor where the actual value of the resistance depends, by the integral reported in Equ. 1.4, over all the currents that have passed through the device. Such "memory" is peculiar for memristors and results from the assumption that the magnetic flux depends nonlinearly on the charge; where this latter assumption is no more valid (so where the $\varphi - q$ curve is a straight line), M(q) is equal to R and the memristor is simply a resistor.

5 yeas after the first paper, Chua generalized the concept of memristors to a special class of non linear dynamical systems called *memristive systems* defined by Equ. 1.5 [5] :

$$\dot{x} = f(x, i, t); \quad v = R(x, i, t)i. \tag{1.5}$$

where x is the state of the system, i , v and t are the current, voltage and time variabilities. Briefly, the meaning behind these latter equations is that the variation of the internal state of the device is a function of the state, the given input and of the time and the memristance has the same dependencies. Moreover, from the memristance definition in Equ. 1.5, the zero-crossing property, according to which the output-input curve has to cross the origin, emerged as the most typical feature of those systems. This is actually what distinguish a simple dynamical system from a memristive one, since for the correct definition of the latter, it's necessary to add the requirement of a zero phase shift where if the input is 0, the output must be 0 . Another typical feature of the memristive systems is the variation of the behaviour of their output-input curves under the application of inputs with different frequencies; more in details, the hysteretic effect of the system is bigger when the frequency is low and it disappears in case of very high value (collapsing into a classical definition of resistor). This new expanded definition of *memristive systems* can be used for the modelling of a large number of systems amongst which the neurons' sodium channel, already described by Hodgkin and Huxley and reinterpretated by Chua in [5]. In 2015 Corinto et al. [6] further extended the concept of memristor introducing the so called *extended memristor* umbrella term, which includes the definition of generic and ideal memristor . Briefly, an extended memristor can be mathematical represented by the following equation (Equ. 1.6)

$$\dot{x} = f(q, i, x); \quad v = R(q, i, x)i; \quad \dot{q} = i \tag{1.6}$$

where q(t) is the current momentum ($q(t) = \int_{-\infty}^{t} i(\tau)d\tau$). From Equ. 1.6 we can obtain the representations of generic memristors (Equ. 1.7) and ideal memristors (Equ. 1.8):

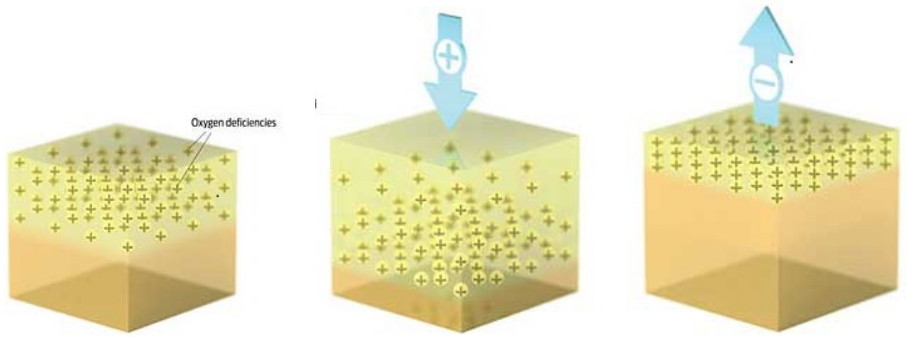

Figure 1.2: *Proposed working principle of the* TiO_2 *memristor [7].*

$$\begin{aligned} \dot{x} &= f(q, i, x) \\ v &= R(q, x)i \\ \dot{q} &= i \end{aligned} \tag{1.7}$$

$$\begin{aligned} v &= R(q)i \\ \dot{q} &= i \end{aligned} \tag{1.8}$$

1.2 FIRST DEVICES

Until 2008, so for the next 30 years, only few papers, mostly theoretic, have been reported regarding the memristive topic. In May 2008, Strukov et al. and the HP lab claimed the realization of a 2- terminal memristor realized as an inorganic nanoscale device, based on the interface between a doped and a stoichiometric layer of TiO_2 [4, 7]. In "the missing memristor found" the working principle of such device was explained with the movement of vacancies from the not- to the stoichiometric region under the application of a voltage (Figure 1.2).

The titania's region with a low content of oxygen is characterized by a lower resistance in respect to the stoichiometric one and the resistance of the entire device results from the weighted sum of the two contributions, where the weights are related to the thickness of the regions.

It is to note that devices of different nature with resistance switching were reported even earlier [8, 9] but they weren't associated to the term memristor. In particular in 2005 Erokhin et al. [8] reported the realization of a hybrid electronic device made of a hetero-junction between a conductive polymer and a polyelectrolyte that presented some typical features of memristor, such as the hysteresis loop in the I(V) curve and an intense rectification property. The chosen conductive polymer was Polyaniline, a well known and studied material, whose typical feature is the wide gap between the resistance in its doped and undoped forms. A brief introduction to the conductive polymers' properties will be the topic of the discussion of the next section.

1.3 INTRODUCTION TO CONJUGATED POLYMERS

In the past, the strong efforts for the study of inorganic materials leaded to the conclusion that such class of solids can behave as semiconductors, metals or insulators depending on their intrinsic properties, while polymers were considered just as insulating materials.

However in the fifties, this notion changed after the discovery of semiconductor properties in a special class of conjugated polymers that, years later (in the 1970s) became even more interesting after the discovery of their conductivities of metallic level. The main characteristic of the conductive polymers is the high conjugation of the backbone with the alternation of single and double bonds in a continuous orbital overlap, that allows the movement of the charge carriers.

1.3.1 Chemical structure: the source of the conductivity

As said before, conductive polymers are characterized by a high conjugation of the backbone in which the alternation of single (σ bond) and double bond (σ and π bond) produces a combination of strength of the chain (due to the σ bond) and delocalization of the electrons along it (due to the overlap of the p-orbitals of the π bond). This phenomenon allows the free and easy movement of the charge carriers along the chain, jumping from one atom to the next one. Moreover, according to the band theory, electrical properties of a material can be deduced from a careful analysis of its electronic structures, attributing it the metal, semiconductor or insulator behaviour [10, 11].

Conductive polymers, in this sense, are no exception since their electronic configuration is made of a bonding (π) and an antibonding (π^*) bands separated by an energy gap. The band gap of conductive polymers has an energy of around 1-4 eV and thus it defines them as typical semiconductors that, exactly as the inorganic case, can be doped for increasing their electrical conduction properties[12].

Although the effect and the terminology are the same for the organic and the inorganic semiconductors, the nature of the doping process is completely different; in the case of an inorganic material the substitution or the inclusion of ions in the lattice are the principal methods in which the material can be irreversibly doped, while for the polymers this result can be archived through a redox or non redox reactions [12].

More in detail, in the first case the reversible oxidation (or reduction) of a conductive polymer induces, with the removing (or the adding) of electrons, the creation of a radical anion, called polaron, in the middle of the band gap[13, 12]. Clearly, a further oxidation or reduction will add charges in the polaron level, generating the bipolaron, by definition spinless, that will significatively

contributes to the conduction phenomenon. In fact this bipolaron formation for addition or removing of the electrons is always accompanied by structural distortions of the lattice that tries to balance the new charge created by the dopant and that can travel along the polymer chain after the application of a voltage.

Another interesting method for inducing the doping process doesn't involve any redox reaction but just the protonation through the use of protonic acids, such as HCl [12]. A widely studied case is the protonation of Polyaniline base form (PANI EB) in emeraldine salt (PANI ES) where, even if it doesn't change the number of electrons in the system, this process is able to induce the rearrangements of the energy levels and the increase of the conductive properties of the material. In fact the conformation of the form undoped (PANI EB) is coiled while after the doping process, the chains are extended basically for the repulsion forces between positive charges. This extended configuration increases the conductivity from $10^{-10} S * cm^{-1}$ of the undoped form to $30 S * cm^{-1}$ typical of the salt form [13].

The first interesting result of this distribution of bands is the so called electrochromic feature of the conductive polymers [14]; by definition an electrochromic material is a material able to change its color in response of different oxidation states. As said before, the typical range for the energy of the conductive polymers' band gap is from 1 to 4 eV so mostly in the visible range; thus the polaronic or bipolaronic level's formation in the middle of the gap induces the modification of the emission spectrum of the organic material, varying the color.

A classical example of this property is the PANI that, with its 3 oxidation states (leucosmeraldine, emeraldine and pernigraniline) and 2 different forms for every oxidation state (protonated or deprotonated form), can vary its color from yellow to purple. Leucosmeraldine is the totally reduced form and in

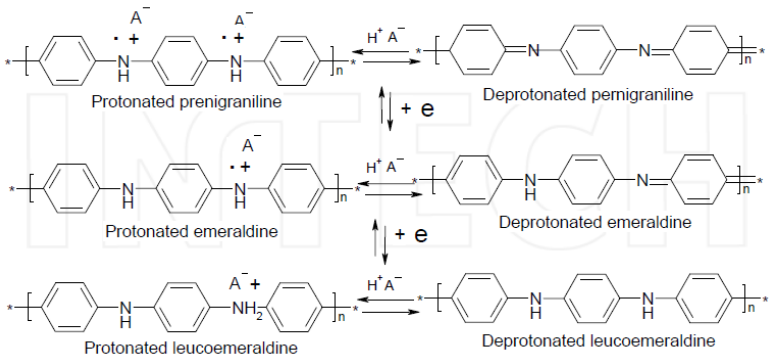

Figure 1.3: *Different forms of the PANI [16].*

its protonated form, it's characterized by a pale yellow color that is extremely different from the purple coloration of the totally oxidated and protonated pernigraniline [15]. The partially oxidated form is the Emeraldine form that is characterized by an intense blue color if deprotonated, or a green hue if protonated. The latter case is the only conductive form of the polymer (Figure 1.3).

1.4 ORGANIC MEMRISTIVE DEVICE

So back in 2005, Erokhin et al. [8] proposed the realization of a three-electrodes hybrid electronic element based on polyaniline –polyethylene oxide/LiCl with rectifying behaviour. The polyaniline chosen for the experiment has a molecular weight of 10000 and it was dissolved in 1 methyl-2-pyrrolidone (NMP) until its concentration reached the value of 0.2mg/ml and the polyelectrolyte was realized with polyethylene oxide (average molecular weight 8000000) doped with LiCl (0.1 M). The current-voltage behaviour obtained was attributed to the electrochemical reactions of the PANI under the solid electrolyte and this was afterwards demonstrated through UV-vis, FTIR and Raman spectroscopies that clarified the role of the ions included in the polyelectrolytes used for the fabrications of the device [17]. Moreover in [18] a further demonstration of

the role of the ions was proposed, taking advantage of a time resolved X-ray fluorescence analysis. In this latter case, Lithium ions were substituted by Rubidium, since the fluorescent energy of the lightest element can't be detected at atmospheric conditions.

Further studies were performed in order to explore different compositions of the conductive channel and of the polyelectrolytes, demonstrating once more the great flexibility of the properties of such devices. In [19] for example, a new functionalization of the conductive polymer (Polyaniline - Dodecyl benzene sunfonic acid-PANI:DBSA) was tested in order to increase the ON-OFF ratio and the conductivity of the device while in [20, 21] the possibility of integrating graphene and gold nanoparticles in the PANI layer was investigated. The role of the polyelectrolyte was deeply analysed [22] comparing different PEO matrix in several ionic compositions. The first important result was the necessity of a high average molecular weight of the PEO since lower ones create a not stable gel, thus making impossible to work with them [22]. The second result was obtained varying the lithium salt inserted into gels. $LiClO_4$, $LiCF_3SO_4$ and $LiBF_4$ were tested and the paper demonstrated, by the acquisition of I-V curves of the assembled devices, that electrical properties are mostly effected by the cation's nature and by the solution's pH respect of the anion's dimensions. This latter assumption is valid if we consider other parameters, such as temperature and humidity, constant and in fact, as reported in [23], variation of working temperature and, as consequence, of the humidity trapped in the polyelectrolyte, deeply affect the device's performances.

Another important aspect that need to be taken in consideration is the nature and the role of the electrodes. In the paper [24] authors deepened the role of the gate electrode substituting it at the beginning with a capacitor and then using graphite.

In [25] authors reported for the first time the realization of adaptive networks based on electrochemical elements, thus demonstrating a strong correlation between the components of the nervous system and their polymeric analogues. In particular, the best candidate for the synapse mimicking was the three-electrodes electronic element reported years before since the main action of the synapse resides in the induction of changes in the signal propagation path, modulating the conduction of this natural junction. A closer introduction to the synapse's world is remanded in the following sections. Moreover, in analogy with the nature where an aggregation of synapses constitutes a neuronal network, the authors reported also the fabrication of an adaptive network realized by means of 8 devices connected with a pairs of input electrodes and a pair of output electrodes. It was demonstrated that starting from a preferential conductive path along the network, this one was can be "re-write" using a training procedure targeted to the suppression of the initial path and the promotion of a second one. After this latter one, other papers [26, 27] reported various applications of the devices in the Hebbian learning mimicking, working for example in pulse mode.

1.5 WHY MEMRISTOR: BIO-MIMETIC AND BIO-INTERFACES

What distinguishes a brain from a computer?

Beside obvious options such as the differences in the constituent materials, the power needed and the ratio between the occupied dimensions and the efficacy, the most impressive answer is that in a computer architecture, processing and memorizing of the information are done separately while in a brain these two process are done concurrently, ensuring the possibility of understand, com-

pare and memorize new items in the same time, i.e. allowing the learning procedure [1] [28].

Moreover in a classical computer, the act of processing and memorizing involves different and separated parts of its architecture (the processor and the memory) that must be called or activated in different times. In the brain, this task is taken by the synapses that are able to adjust and adapt their synaptic weight ensuring to the biological systems the possibility of performing learning operations [28]. The same kind of adaptivity is actually present in different living system and in particular it was studied by Zhang et al. using the protoplasmic networks of slime mould "Physarum polycephalum" for the realization of a novel algorithm for a supply chain design[29, 30].

Furthermore, the large connectivity between neurons (10^4 in mammalian cortex) is responsible for its extremely high efficiency in term of parallel processing power [31], fact that a standard von Neumann architecture with its physical limits cannot satisfy. In the next section, a brief introduction on the synaptic properties will be given.

1.5.1 Synapses

The word "synapse" originates from the Greek συναψισ, meaning "conjunction", introduced in 1897 by the English neurophysiologist Charles Sherrington in Michael Foster's Textbook of Physiology for describing a structure that permits a neuron (or nerve cell) to pass an electrical or chemical signal to another neuron [32]. A synapse in fact is made of two parts: the membrane of the signal-passing neuron (the presynaptic neuron) and the membrane of the target (postsynaptic) cell separated by a gap (named the synaptic cleft) of 20-40 nm in case of chemical synapse and of 3.5 nm in case of an electrical one [33].

1 http://scienceblogs.com/developingintelligence/2007/03/27/why-the-brain-is-not-like-a-co/

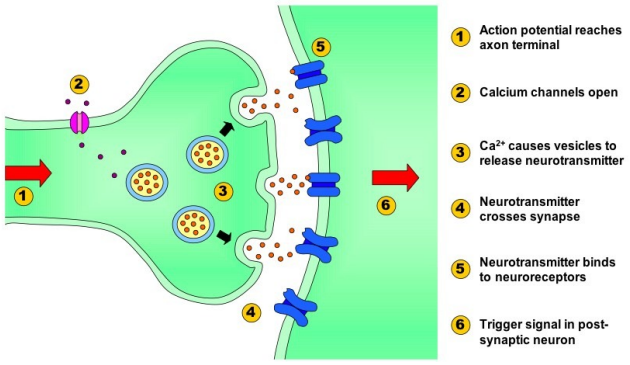

Figure 1.4: *Synaptic trasmission's steps*

In a chemical synapse, the transmission of the signal between two neurons is a process that involves the entire bodies of the cells and it starts when the wave of electrochemical excitation, called action potential, reaches the synaptic site. Due to the voltage variation, it causes the electrical depolarization of the membrane that is forced to open the channels allowing the permeability of calcium ions. This activates the opening of some vesicles containing neurotransmitters into the synaptic cleft where the neurotransmitters diffuse and then reach chemical receptor molecules located on the membrane of the postsynaptic cell. At this point, the binding between the molecules and the receptors activates the new neuron and the transmission process continues in the next neuronal cell [33](Figure 1.4).

The efficiency of the transmission process described above is effected by the previous activity of the synapse and more in detail the increase or the decrease of the synaptic activity induces a strengthen or a weaken of the ability of synapses of transmit the "chemical" signal [34]. This property of evolving in time of the synapse's strength is called *synaptic plasticity* and it is considered as one of the most important neurochemical foundations of learning and memory on which the well known Hebbian theory is based on:

When an axon of cell A is near enough to excite a cell B and repeatedly or persistently takes part in firing it, some growth process or metabolic change takes place in one or

both cells such that A's efficiency, as one of the cells firing B, is increased [35].

Moreover the synapse plasticity can be effected by the morphology of the synaptic conjunctions and can be described in terms of homosynaptic (occurring at a single synapse) or heterosynaptic (occurring at multiple synapses) [33]. In the first case any variation of the synaptic strength is due to the past activity of the synapse and it's input-specific, meaning that any reinforcements or depressions occur only between the specifically stimulated post-synaptic target and the pre-synaptic part [36]. Homosynaptic plasticity and input specificity together with the so called associativity (the increase of the synapse's strength in case the pre- and the postsynaptic neurons firing are correlated in time) constitute the modern definition of the Hebb rule [36, 37, 38].

On the other hand, the heterosynaptic plasticity [39] instead doesn't have the requirement of the input specific connection and the efficacy of a synaptic connection between a neuron and its target can be altered by the action of one or more neurons not included in the former channel. Moreover, modifications that occur in the synapse can be effective for a short-term (STP or STD), including the so called synaptic fatigue and synaptic augmentation, or for long-term, i.e. long-term depression (LTD) and long-term potentiation (LTP) where pulses of electrical stimuli are addressed to the synapse for depressing or potentiating its synaptic response, respectively [33].

1.5.2 Neural network

All the concepts described in the previous section are related basically to the properties of a single synapse and must be considered as the building blocks of a more complex system in which neurons aggregate to form networks. In this new system the description of transmission of the signal need to be slightly

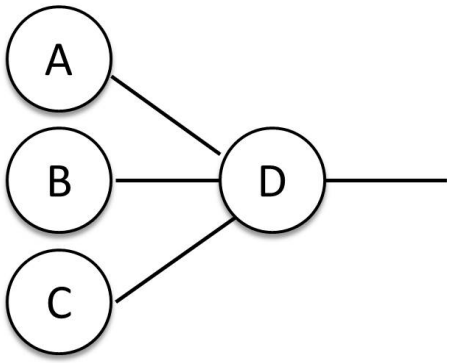

Figure 1.5: *Scheme of a neural network: circles are neurons and lines are synapses.*

implemented in order to include also the contribution of all the other neurons and connections that surround the given synapse. Looking at the scheme of a neural network reported in Figure 1.5, the single transmission of the signal (described in the section 1.5.1) between neuron A and the neuron D is paired with the transmissions of different neurons (B and C) to the neuron D [40]. All the contributions are summed [33] and if the resulting value exceeds a threshold potential, the cell D will carry out all the steps necessary for the further transmission, starting from the opening of the sodium channel and finishing with the firing.

The combination between the summing process and the threshold potential is necessary for the correct firing of the neurons since it ensures that the contributions of both excitatory and inhibitory neurotrasmitters modulate the activity of the receiving neuron, excluding the "spontaneous" firing of the cell if not stimulated [33].

1.5.3 Bio-mimicking: memristors as synapse analogues

Roughly speaking, a synapse is essentially a two terminals device whose main feature is the ability of change its efficiency in response of different stimuli that the two neurons receive and have received in the past. This characteristic is

also the principal reason why memristors in general, and organic memristive devices in particular, are the best candidates for the mimicking of the activity of the synapses [31, 41, 42, 43]. In fact, similar to their biological counterpart, memristors can vary their memconductance in response of previously received stimuli, providing both the plasticity and the connectivity necessary for the realization of a biological neuromorphic circuit[31]. Moreover in respect to the external circuit, organic memristive device is a two terminals device since the third gate electrode is just a reference electrode and so the analogy with the synapse is even stronger.

This idea directly comes from the already mentioned Chua's paper [5] of 1976 where he described as one of the possible applications for memristors the memristor model for the Hodgkin-Huxley neuron.

Snider [44, 45] proposed in 2007 to exploit the dynamical characteristic of the "crummy" memristive devices using them for the realization of self-organizing networks for the implementation of massively parallel computations instead of using them as nanoelectronic systems. This change of perspective was the base for the realization of cheap adaptive networks, in which the use of pulse (spike)-based communication ensures a sufficient processing speed but in same time a moderate power consumption. Moreover, the use of such kind of pulse paved the way for the application of the memristor in the field of the neuromorphic implementation of the learning rule known as Spike Time Dependent Plasticity (STDP)[45].

As reported before, the Hebb rule is based on the synaptic plasticity that correlates the synaptic weight's changing with the firing rate of the neurons that compose the synapse ("those that fire together, wire together") [35]. In the STDP mechanism the directionally of the synapse is taken into account describing the synaptic weight's modification in term of the relative time between the fire of the presynaptic part and the postsynaptic one [46, 47, 48]. A synapse

will be potentiated if the presynaptic neuron fires before the postsynaptic neuron while in the opposite case, the synaptic link actually gets weaker. The implementation of the synaptic plasticity can be archived in one hand realizing elements able to satisfy the learning rules previously described or realizing group of devices, collected in circuit or arrays [49, 50, 51], in which the total output of the system must satisfy the learning algorithms. Jo et al.[31] realized in 2010 a crossbar array of devices made of a layered structure of Ag/Si capable of varying the total conductance of the array in response of voltage pulses applied between the electrodes.

In the recent paper of Saighi et al. [43] different implementations of STDP are reported taking advantage of the device physics of different memristive (Spin-Transfer Torque Magnetic Tunnel Junctions , ferroelectric tunnel memristor, Ferroelectric Resistive Switching Memristors) devices together with short term plasticity and short term and long term plasticity.

In the same direction is the work of Kavehei et al. [52] with the additional consideration that even a single memristive device can implement STDP and as a consequence also LTP and LTD. The implementation of LTP or LTD mechanism was the object of study of different groups [53, 54, 55, 56] in which a particular highlight must be done to the work of He et al. [56] that using an inorganic memristor were able to induce both LTD and LTP varying the frequencies and the polarity of the input pulses, mimicking the biologic synaptic behaviour. Moreover, Ohno et al. reported the possibility of switching between Long Term and Short Term Potentiation in a memristive device based on the filament formation of Ag between electrodes [54]. What this group reported was the dependency of the synaptic conductivity and the transition between STP and LTP on the spike rate. In fact in a low frequency regime, the filament tends to relax between pulses and it doesn't reach the critical size for maintaining the conductive state, while a higher frequency lead to a strong filament that

maintains the device in the ON state. In the same direction Chang et al[55], reported the same transition between STP and LTP using an inorganic memristor based on WO_3.

A significant further step toward the realization of a neuristor was reported in [57] where the group of Williams described the fabrication of a memristive circuit able to emulate the action potential generation and propagation including the "all or nothing " threshold action, the refractory period and the constant propagation velocity and wave shape. Recently, Bennett et al. [58] reported the realization of crossbar arrays for supervised learning with organic memristor devices made of a thin film of tris-bipyridine iron complexes (TBFe) where the working principle is based on the formation of a conductive filament in the polymeric film under the application of a positive bias. It's to note that even if the name of organic device is the same for this latter case and the organic memristive devices realized in the Erokhin's group, the working principle and the properties of the two kinds of devices are rather far away. The Bennett's results show clearly that in order to switch on the device it is necessary to apply a voltage value of 3-4 V while to bring it to the high resistance state, the voltage must be doubled. Electrochemical memristors instead present a voltage working range a lot more restrained since the ON state is induced with the application of 0.6 V while the OFF state with -0.1V.

Most of the papers cited since now describe the use or the theoretical model for memristive devices in which the working principle is based on filament formation or ions movement. In addition, all the works regarding the neuromorphic applications of memristors seem to exclude the role of the heterosynaptic plasticity, focusing more the attention on the hebbian definition of synapse. Just one paper [59] reported the fabrication of a 3 terminals device, with a geometry similar to a transistor, in which 2 of them conjunct the conductive channel while the third acts as a modulation electrode.

The first part of this thesis is to be inserted in this scenario, aiming to describe and find out possible neuromorphic applications of electrochemical (organic) memristor devices, taking into account also the heterosynaptic contribution.

1.5.4 Perceptron: a brief introduction

As said before, one of the most important features of the brain is the great parallel processing power due to the big connectivity between its units i.e. neurons; This parallel distributed processing has been emulated in the so called artificial neural networks (ANN) in which the informations processing is inspired to the neuronal connectivity. In such kind of network, mathematical simplification of biological neurons and synapses are represented typically with spheres units for the first and lines for the latter; to the synaptic connection is associated the parameter w_i that represents the synaptic strength and acts as weight vector for the ith input.

Moreover an ANN is often organised in layers for example input layer in which the input signal is addressed or the output layer in which the final result is acquired.

Different connection's geometries between neurons are possible and they deeply affect the final performances and properties of the network. For example the direction of the information moving (as result of restrictions given to the ANN) classifies the networks in Feed-forward network in which the information moves only in one direction (from the inputs to the outputs layer) and the recurrent neural networks in which every unit is both an input and an output (Figure 1.6).

In the first class of networks find place special subclasses named the single and the multiple layer perceptrons that differ one to the other for the number of layers between the input and the output: in the case of a multilayer (let's

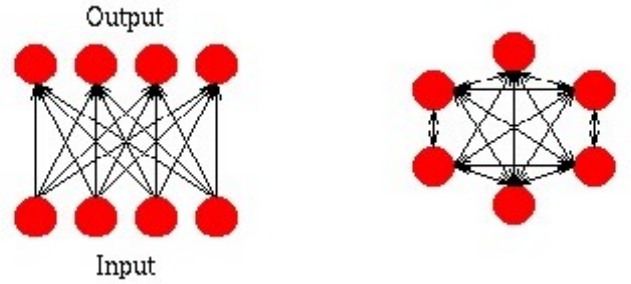

(a) *Feed-forward network.* **(b)** *Recurrent neural networks.*

Figure 1.6: *Feed-forward network vs Recurrent neural networks .*

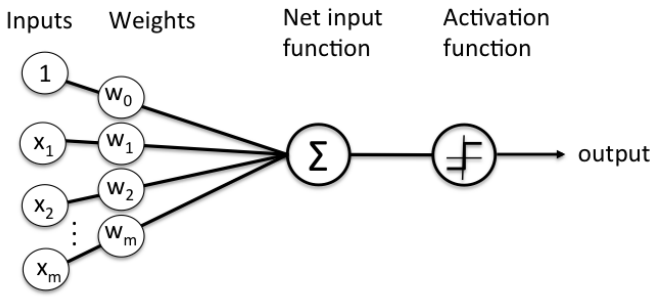

Figure 1.7: *Perceptron's scheme*

say double) perceptron there is a layer called hidden layer, while in the case of a single perceptron it's absent. In machine learning, the perceptron is an algorithm, dates back to the 1950s [60, 61], for supervised learning of binary classifier since it can distinguish if a certain given input belongs to a specific class or not. Moreover it's defined also as a linear classifier, since it makes a classification decision based on the value of a linear combination of the input with the set of weights w_i.

Associated with each layer there is the so called "transfer function" composed by a "net input function" that applies a baseline to the value of the linear combination and an "activation function" that is applied to the net input.

The simplest activation function is the threshold one (like the Heaviside step) that has as possible outputs just two values for all the inputs (Equ. 1.9).

$$H(n) = \begin{cases} 1 & \text{if } n>0 \\ 0 & \text{otherwise} \end{cases} \quad (1.9)$$

Looking at Figure 1.7, we can conclude that the output of this network is therefore resulting from $\sum_i w_i x_i$ plus the bias $+b$ given by the net input function and the "separation" in two values by the threshold activation function. Putting all together we can write the output value of f(x) as (Equ. 1.10):

$$f(x) = \begin{cases} 1 & \text{if } \sum_i w_i x_i + b > 0 \\ 0 & \text{otherwise} \end{cases} \quad (1.10)$$

This latter one (Equ. 1.10) is the equation that describes the working principle of the perceptron. In other words, a perceptron is a function that maps the inputs (a real-valued vector - $\overline{x}$) to a single binary output value f(x) whose possible values are (0 or 1) . If the value of x_i satisfies the first case of Equ. 1.10, then the f(x) will be 1 and the perceptron will classify the input x_i in the class 1. Otherwise x_i will be inserted in the class 0.

Now, since this is also an adaptive network, we need also to include the possibility of varying the response of the input classification to drive it for our need and the only way to perform it is to admit that the weights w_i can vary in time ($w_i(t)$). But, as we said before, these weights represent the synaptic strength thus we can use the biological terminology for describing the increase of the strength as the potentiation process or its decrease as the depression. Moreover these two processes must be done following some specific learning algorithms, among which the backpropagation method, error correction and the delta rule one are the most common. The first one is the most complex and it's suitable for the implementation of the double layer perceptron because

it can take into account the extra hidden layer of the scheme. The other two instead are useful only in the case of the single layer perceptron.

The error correction is the simplest of the three methods proposed and it provides the variation of the weights depending only on the sign difference between the desired and the actual output [62].

The plasticity and the working principle of the perceptron make it the best candidate for the mathematical model of the firing of biological neurons, being able to mimicking the threshold function that characterizes these kind of cells [63].

For this reason, with the intent of providing a complete representation of the neuromorphic possibilities of the organic memristors, a part of the thesis will be focused of the hardware realization of the single-layer and a multi-layer perceptron.

1.5.5 Bio-interfacing: memristors as artifical synapses

The use of the organic material based devices for bioelectronics applications can present some interesting advantages respect to the classical passive metal electrodes [64]. The possibility of detecting low concentrations of biological compounds and low output brain activity with such kind of devices matches the necessity of provoking less damages than is possible. Furthermore, the most promising technology on this field are the organic electrochemical transistors (OECTs) in which a PEDOT:PSS channel in connected with two electrodes at the edges and through a liquid electrolyte to a gate electrode [64]. The main uses of the OECT have been demonstrated in the field of sensing ions content [65], ions nature[66] and pH local variations [67] and moreover in the field of recording the electrical properties of nonelectrogenic and electrogenic cells [64]. Neuronal cells reside in the last class of cells and the use of OECT ensures the

possibility of amplify the signals, providing a high value of transconductance. In other words, the work of the Malliaras' group described above can be resumed saying that the main application for organic devices is the sensing of chemical variabilities variation or the recording of the activity of different cell lines in which the transistor play the role of an "electrode" with amplification properties.

The work presented in the last part of the thesis, instead, is even more ambitious of the previously sections, betting on the possibility of integration of a neuromorphic synapse analogue (the memristor) with real and living neuronal cells. In this case, the action of memristive devices can not be reduced just to complicate electrodes but plays also the active role of a synapse, modulating its conductive properties in function of the input signals received.

After this brief introduction to few basic concepts regarding the memristor's properties and some hints on the biological and the device's aspects of the mechanisms involved in the implementation of the neuromorphic functions, this thesis will be articulated in two main parts in which the results obtained in the realization of memristive devices able to perform features of the synaptic plasticity are presented together with the results of the direct interfacing of the organic memristor with different cells. More in detail, the first part of the results are presented following the order given by the system's degree of complexity: the initial results, in which we implemented typical features of the homosynaptic plasticity, such as the Long Term Potentiation (LTP) and the Long Term Depression (LTD), were obtained using a single device; subsequently the geometry of a standard device was gently modified for adapt it to the implementation of the heterosynaptic plasticity; furthermore exactly as happen in biology were a group of single unit cells forms a network, we realized artificial neuronal networks (ANN) in which the main role was played

by memristive devices. The accomplishment of an elementary perceptron and, afterwards, of an ANN that can be considered as a precursor of the double layer perceptron, were reported. The final part of the thesis is focused on the interface between the neuronal cells and organic memristive devices and it's divided in an initial steps in which we tested the bio-compatibility of the polymeric main component of the devices, and the final step in which we reported evidences of the possibility of connecting two nervous cells through an organic memristor preserving their biological communication mechanisms.

2 MATERIALS AND METHODS

Contents

2.1 BUILDING AN ORGANIC MEMRISTIVE DEVICE

First publications of memristor based on organic molecules have been reported since 2008 [68, 69, 70] even if 3 year before the paper entitled "Hybrid electronic device based on polyaniline-polyethyleneoxide junction" was already printed [8] and described the realization and the features of a device, not identified as memristor, but with some features of "memristor" of Widrow [71] and the same properties of Valentino Braitenberg mnemotrix element in his mental experiment explaining learning [72].

Organic memristors are characterized by a channel made of conductive polymer. In our case the polymer is Polyaniline, PANI, that is deposited on the substrate by the Langmuir–Schaefer (LS) technique.

2.1.1 Architecture and preparation

Briefly, in the LS technique, a monolayer called the Langmuir film is fabricated at the air-liquid interface with a control over the surface pressure of the molecules density. For our samples the liquid, the subphase, is demineralized-deionized water prepared with a Milli-Rho-Milli-Q system. Touching the monolayer with a solid surface (the substrate), the Langmuir film is transferred to it and, depending on its orientation, it is possible to distinguish the Langmuir-Blodgett and the Langmuir-Schaefer Technique. The latter is characterized by a horizontal deposition [73], while, in case of Langmuir-Blodgett, the substrate touches the surface perpendicularly .

For more details about the Langmuir-Schaefer Technique see the section "Langmuir Blodgett films" in A.1.

The solution used to fabricate the Langmuir film is prepared in 1-methyl-2-pyrrolidinone (NMP, GPR Rectapur VWR) with 0.1 mg/mL of polyaniline emeraldine base (Sigma Aldrich) and 10% of Toluene (Normapur, VWR) [74]. This preparation is filtered twice with PTFE filters with porous membrane of 0.45 µm and injected on the water subphase and the polymeric chains are then compressed until reaching the target surface pressure of 10 mN/m. Subsequently, the monolayer obtained is separated into sections with a special grid that cut it in smaller films and finally deposited for Langmuir-Schaefer Technique on a glass insulating support with two evaporated Chromium electrodes. In our standard devices the most performing thickness of the active polymeric channel is obtained with the deposition of 60 layers (approx 100 nm) of conductive polymer (PANI) (approx. 5x15 mm) in order to combine the necessities of good conduction properties and a rapid diffusion of the lithium ions in the conductive polymer. In this sense, the combination of a coloured polymer and the Langmuir-Schaefer technique give us the possibility to control the thickness

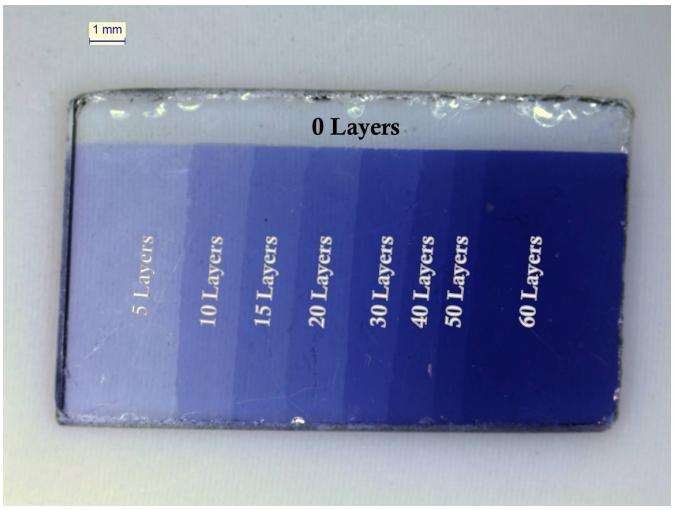

Figure 2.1: *Example of Langmuir-Schaefer deposition method*

of the polymer directly during the deposition process, increasing or decreasing the number of monolayers deposited. The accuracy of the process is in term of nm since the thickness of a monolayer of PANI is estimated in 1-2 nm [75]. A demonstrative example of the potentiality of the technique is reported in Figure 2.1 where different thickness of PANI are deposited, from 5 to 60 layers.

The polyaniline used for the deposition is in its undoped form that is characterized by an intense blue color and a low conductive proprieties (i.e. its insulating form). In order to enhance the conductivity, it's necessary to treat the channel to induce the necessary protonation (described in 1.3.1 on page 7) dipping it for 40 seconds in HCl 1M (AVS TITRINORM, VWR) to dope the polymer to the emeraldine salt conducting form. At this stage, after the transition, two major effects are evident: a chromatic variation (from blue to green) and a strong decrease of the resistivity of the channel; while from a compositional and morphological point of view, it's possible to observe other small, less evident, variations of the film properties such as the rearrangement of the nitrogen bonding and a moderate decrease of the sample's thickness. This was possible by means of the XPS and AFM techniques respectively and will de discussed in the following sections (Section 2.3 on page 33).

After about 40 minutes, this doping process is repeated for just 20 seconds to stabilize the film conductive properties. A water solution of Polyethylene oxide (PEO, Sigma Aldrich) with a molecular weight of $8 * 10^6$ Da is prepared with a concentration of 20 mg/mL and doped with 0.1M $LiClO_4$. Lithium ions in such configuration co-ordinate four-five oxygen atoms belonging to one or more polymeric chains from one polymer chain to another and they can move in the network following the three-dimensional hopping model with varying barrier heights.

This water solution is left overnight to induce a natural solubilization of the long chain polymer and the total gel formation; once that the gel is formed and homogeneous, it can be used as a solid electrolyte, depositing it on the PANI channel in a crossed configuration. After the complete drying of the gel, a silver wire (0.05 mm, GoodFellow) is inserted in this first layer of PEO and fully covered with another stripe of polyelectrolyte. The contact area formed by the interface of between PANI and PEO is named the *active zone*, since this is the area of the conductive polymer that is going to undergo to all the redox reactions responsible for the conductivity variations of the device. In this sense, the silver wire used as reference electrode, gives use the possibility to keep track of the electrochemical reaction in the area. The final structure (reported in Figure 2.2) is further doped with HCl vapors [74] to offset the pH variation induced by the application of the polyelectrolyte gel after the deposition.

The two Chromium electrodes, present under the PANI channel are defined *source* (S) and *drain* (D) electrode while the silver one is the *gate*.

The working principle

As said before, the working principle of the device is based on the redox activity at the interface between PANI and lithium doped PEO. Since polyaniline has 3 different oxidation states[76, 77] the redox reactions potentially involved

are two: from leucosmeraldine to emeraldine salt (and viceversa) and from emeraldine salt to pernigraniline. The latter one must be discarded since it's an irreversible reaction and thus, after the complete overoxidation of the PANI, it would not be possible to re-obtain the emeraldine form. Thus the only possible reaction for our application must be the first one and to avoid the overoxidation is necessary to not exceed, in the positive part of the voltage working range, the value of 1.5 V. The reported values for the oxidation to the emeraldine and the reduction back to the leucosmeraldine of the PANI are 0.3V and 0.1V [76, 77] but, in our working device, we need also to take into account the voltage distribution along the channel. More in detail, the differential potential applied to the conductive PANI channel between the S and D electrodes will have a linear distribution from the lower potential (ground) to the upper potential (Voltage value). This means that, in a simplistic configuration, in the middle of the channel the effective potential is more or less the half of the applied potential (Figure 2.3) .

Clearly, if we want to induce a reaction we need also to take into account this scaling factor and use a wider voltage range. A sketch of the device's working principle is reported in Figure 2.4.

Right after the fabrication (Figure 2.4 a)), the device is in its ON state, characterized by the PANI emeraldine salt form and thus a high conductivity. After the application of a negative voltage, the PANI channel undergoes a reduction

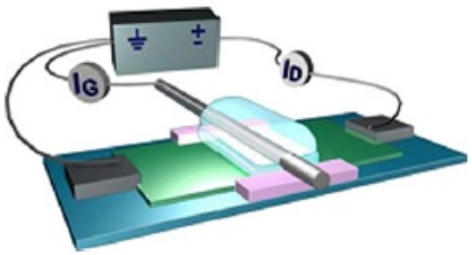

Figure 2.2: *Scheme of an organic memristor: PANI active channel in green; solid polyelectrolite in light blue; chromium electrode and silver wire in gray. Reprinted with permission from [74].*

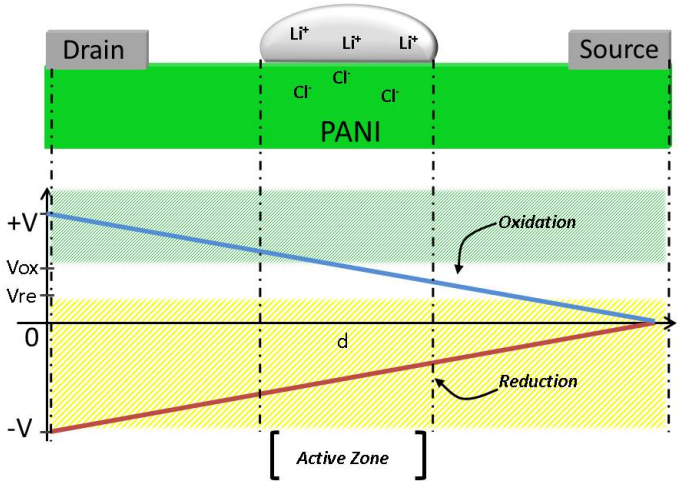

Figure 2.3: *Voltage distribution along the device: panel a) a sketch of the memristive device; panel b) applied voltage (±V) vs the distance between electrodes (d): potential distribution along the channel in the case of reduction (red curve) and oxidation (blue curve) mechanism. Two areas of the graph are highlighted: the oxidation are in green and the reduction area in yellow.*

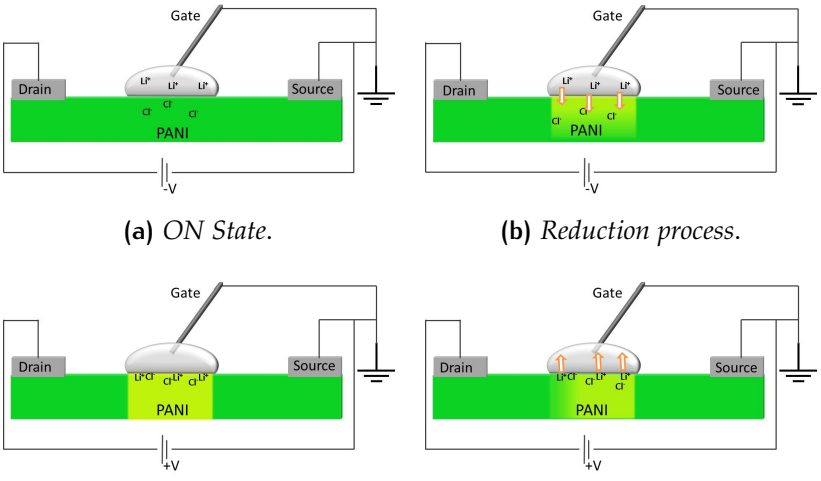

(a) *ON State.* **(b)** *Reduction process.*

(c) *OFF state.* **(d)** *Oxidation process.*

Figure 2.4: *Proposed working principle of the PANI memristor.*

process that end with the device in its OFF state (Figure 2.4 b)). This process is relatively fast since, thanks to the voltage distribution shown in Figure 2.3 (red curve), all the active zone feels the effect of a potential lower than the reduction voltage (Vre in the figure). Once that the PANI is reduced, applying a positive voltage higher than 0.3V, it's possible to induce the oxidation process. This latter one is slower that the previous since the potential that the active zone feels is not homogeneously higher that the oxidation voltage, thus just part of the area undergoes the reaction (Figure 2.4 c)). Gradually the distribution along the channel changes until the complete oxidation of the active zone and the reset of the ON state is archived (Figure 2.4 d)).

The working principle of the device can be written following the reaction reported in [8]:

$$PANI^{+} : Cl^{-} + e^{-} + Li^{+} \rightleftharpoons PANI + LiCl \tag{2.1}$$

where $PANI^{+} : Cl^{-}$ represents the emeraldine salt form after the doping in HCl and PANI the leucosmeraldine. The two forms present differences in conductivity of orders of magnitude and the mechanism proposed here for the conductivity switching was deeply confirmed by microRaman spectroscopy [17] and X-ray fluorescence [18].

2.2 DEVICE CHARACTERIZATION

2.2.1 Electrical characterization

In a standard characterization two currents are considered: the ionic current flowing through the reference electrode (gate current: I_G) and the total current

passing between source and drain (source-drain current: I_D),acquired respectively Keithley 6514 multimeter and Keithley 236 source measure unit. These two Keitheley are connected to a computer and controlled by an ad hoc matlab's software.

For our standard characterizations is extremely important to connect the two measuring instruments and the device with a specific circuit. Source and Drain electrodes must be connected to the source measure unit in which one of the two is grounded and the gate electrode must be grounded too, in order to guarantee the correct voltage distribution along the channel and at the interface of the active zone. I_D, in fact, results from the sum of both the ionic and the electronic current contributions and so, in order to estimate the correct electronic properties of the device, we report the electronic current (I_{DIFF}) resulting from the algebraic difference between I_D and I_G. Typically, a voltage sweep is applied between S and D following a triangular shape (from 0.0V to 1.2V; from 1.2V to -1.2V and then from -1.2V to 0.0V) with steps of 0.1V for 1 minute. This cyclic characterization is the first necessary step for the determination of the working range of the device and it's paired to a dynamical kinetic characteristic obtained fixing a voltage value applied between the chromium electrodes and acquiring the currents every 1s. This latter characteristic is important for the understanding of the time response of the device and tells us informations about the kinetic transition between the ON and OFF states.

These former characterization implants are based on the fact the polyelectrolyte is kept grounded by the gate electrode and every variation in the conductivity of the device is induced by the different potential given at the source-drain electrodes. So, even if we use the FET (Field Effect Transistor) terminology, the standard *modus operandi* of a memristor is rather different from the transistor's one. However, recently we exploited for our devices the transistor operation mode in which the gate electrode is not necessarily grounded but

can modulate its voltage in a certain range. For such experiment we took advantage of a different set up using two Source Measure Units NI PXIe-4138/9 and also equipped with a multifunction DAQ NI PXI-6289 both driven by a dedicated Labview software.

2.2.2 Optical characterization

We took advantage of the electrochromic features of PANI to detect the memristor's switching without any additional electronics by means of a spectrophotometer, well described in [78], acquiring the reflectance spectra of the memristor at different bias. Briefly, the spectrophotometer is made up of a transmission spectrometer (Imspector V8, Specim, Finland) designed for covering the $400 \div 780$ nm spectral range with a spectral resolution of about 2 nm and coupled to a monochrome 2/3 inch CCD matrix chill digital camera (Hamamatsu C4742-12bit, 1280x1024 pixels, 9 f/sec). The illumination is obtained by means of two 150 W halogen lamps that produce an illuminance of about 30000 lux in a horizontal light band 5 cm high. Finally, a software program control and drives the scanner, acquiring data of a strip of the sample and calculating the CIE color coordinates.

2.3 MORPHOLOGICAL AND COMPOSITION CHARACTERIZATION OF THE PANI FILM

Moreover, in the aim of interfacing PANI memristors with living cells, we further characterized film made of 48 layers of polyaniline emeraldine base and polyaniline emeraldine salt form by means of X-ray photoelectron spectroscopy

(XPS) using a Scienta ESCA200 instrument equipped with a hemispherical analyzer and a monochromatic Al Kα (1486.6 eV) X-ray source, in transmission mode (the emission angles were 90°) [79]. Such kind of configuration ensures the acquisition of informations coming from approximately 10 nm of the sample and different core lines were tested (Si2p, O1s, C1s, N1s and Cl2p).

Furthermore, the morphology of the prepared samples was analysed by AFM characterization (shown in Fig. Figure 3.39) (Cypher AFMsystem (AsylumResearch, Santa Barbara, CA)) in AC mode in air and the film thickness was estimated by mean of a P-6 profilometer (KLA Tencor, USA).

3 RESULTS

Contents

3.1 ELECTROCHEMICAL DEVICES

Typical electrical characteristics of the organic memristive device are presented in Figure 3.1 in which the most important feature is the strong correlation between the behaviour of the ionic (I_{GATE}) and of the electronic current; in fact they represent two complementary ways for characterizing a memristive device.

In the initial part of the scan, from 0 V to 0.5 V, the active zone is totally reduced, thus non conductive, and its insulating properties result in a low

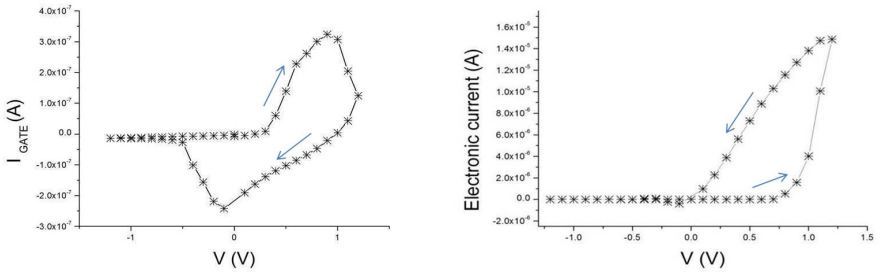

Figure 3.1: *I(V) curve of gate current (left) and electronic current (right).*

electronic current value (I_{DIFF}) in all the device. When the voltage reaches the value of 0.6 V, an intense peak appears in the ionic current, demonstrating the occurred oxidation of PANI; this variation affects the electronic current that, at the same voltage, starts to increase until it reaches the maximum slope of the I-V curve where the active zone is totally conductive and the device is in its ON state.

During the voltage back-scan, the electronic current presents values higher than the ones previously measured for the same applied voltages and this leads to the formation of the typical hysteresis loop in the current curve of memristive devices. Passing the 0 and reaching the value of -0.1 V, the ionic current presents a negative peak that corresponds to the reduction of the polyaniline and to a significative variation of the I_{DIFF} that returns in the regime of high resistance.

3.1.1 Developping an anternative characterization

The polyaniline's redox reaction from non-conductive leucoemeraldine form to the conductive emeraldine salt form (and vice-versa) is always accompanied by the chromic variation from yellow to green (and vice-versa) [80]. This transition occurs in the device's active zone[81] upon the application of a proper voltage and leads to the color changing shown in Figure 3.2.

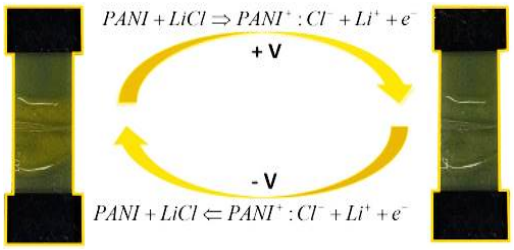

Figure 3.2: *Electrochromic features of PANI: color changing in the active zone of the device associated to the redox reactions of the conductive polymer [82] .*

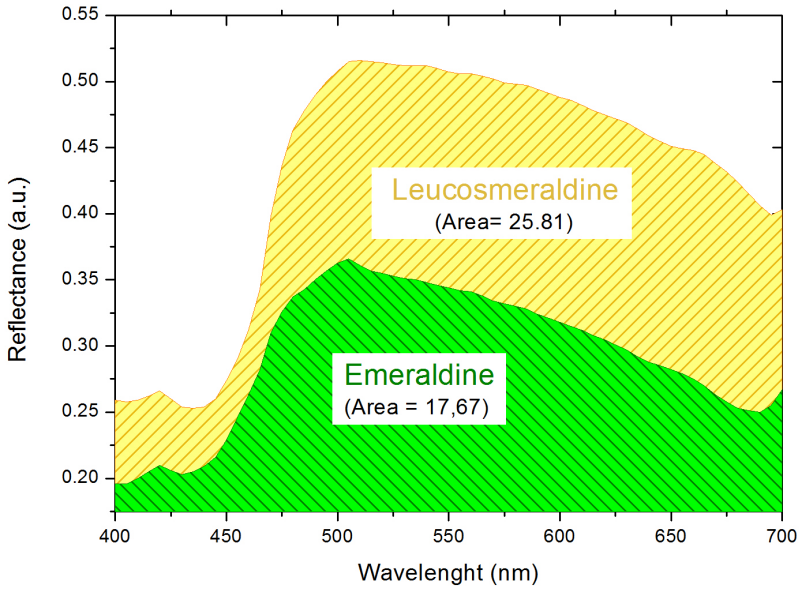

Figure 3.3: *Reflectance spectra measured when the active zone was in the two different redox states. We highlighted and calculated the areas under the two curves [82] .*

Beside the immediate evaluation, we wanted to quantify the color variation between the ON and the OFF states of the memristor, estimating it by means of reflectance measurements (equipment details are reported in section 2.2.2 on page 33) of the two different optical behaviours of the PANI oxidation states. Results reported in Figure 3.3 show that their reflectance profiles differ from the shape and moreover by the area underneath the curves. The emeraldine salt in fact presents a broad peak centered in 510 nm, while the leucosmeraldine has a big broad band above 550 nm. If we compare with literature [78] the two measured forms, they clearly correspond to two different colors: the oxidated form of PANI is an intense green, while the reduced one is yellow, as expected [82]. We have also estimated the areas under the two curves (values are inserted in Figure 3.3) the result of which are rather different from each other (the area calculated from the leucosmeraldine form is bigger of $\approx 40\%$ than the emeraldine one).

Therefore, the electrochromic features of PANI seem very useful for the developing a new and non-invasive method for the characterization of the memristive devices since, as said before, the transition between the ON and OFF state of the memristor is always accompanied by a chromatic variation of the polymer that can be detected using optical techniques, without any additional electronics. For that purpose, we realized a standard device with the same materials and procedure reported in [82] on which we performed spectrophotometric analysis (details in section 2.2.2 on page 33) while biasing it to different voltage values by means of a source-meter, thus monitoring the temporal variation of the reflectance spectra during the inducted redox reactions. In our set up, described in section 2.2.2 on page 33, a single optical measurement requires 1 min and we recorded one spectrophotometer image each 120 s. In the meanwhile we applied with a 236 Source Measure Unit (Keithley) a DC voltage of $+0.8V$ for 22 min to induce oxidation of PANI and, after, $-0.1V$ for 16 min to

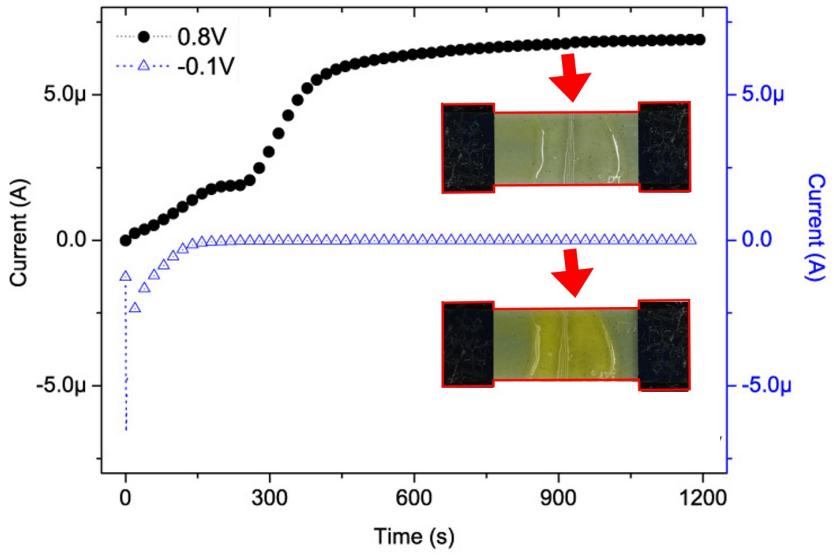

Figure 3.4: *I(t) curve for different applied voltage: black dots for 0.8V and blue triangles for -0.1V; in the inset the chromatic variations of the active zone.*

induce its reduction. In Figure 3.4 beside the electrical behaviour of the device in response of two different applied bias, the final output of the chromatic variation of the active zone is presented as inset of the relative reaction. During the negative bias (blue curve), the current reaches saturation after only 180 s, while, in case of positive polarity (black curve), the conductivity increases slowly and reaches the saturation after 400 s.

In order to compare the electrical curves with the optical spectra we decided to represent the optical transition by plotting the area of the reflectance spectra versus time for both the redox reactions (Figure 3.5 a) and Figure 3.5 b)) [82] .

As it is shown in Figure 3.5 a) and b), two different areas of the active zone (*Zones* 1 and 2) follow the same trend: in the case of reduction the areas under the spectra tend to increase in time (Figure 3.5 a)) and to decrease in the case of oxidation (Figure 3.5 b)). It's to note that both curves of Figure 3.5 confirm the saturation time observed in current characterization of Figure 3.4.

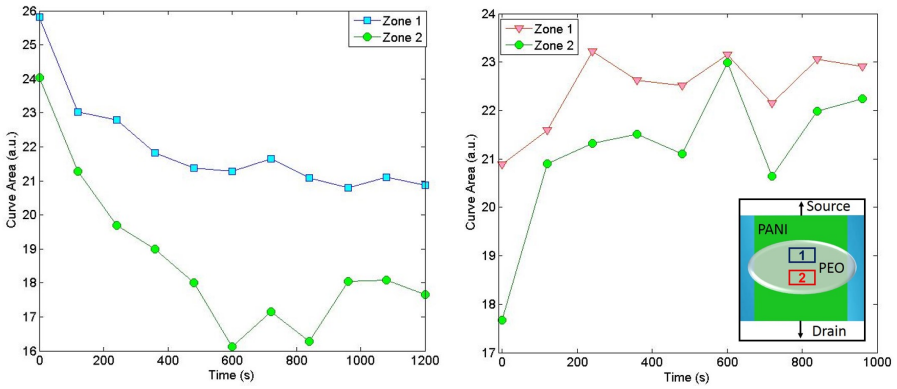

(a) Oxidation **(b)** Reduction

Figure 3.5: *Area of the reflectance spectra versus the time for the redox process: panel a) oxidation process (0.8V) and panel b) the reduction (-0.1V). Inset of panel b) Scheme of the memristor's active area divided in two zones. Blue rectangle for* Zone 1*, closer to the grounded electrode (Source) and red rectangle for* Zone 2*, closer to the biased electrode (Drain) [82] .*

Moreover the most satisfactory function for fitting the two areas curves is an exponential function of the form:

$$y(t) = y_0 + A * \exp(t/\tau) \tag{3.1}$$

where y_0, A and τ are parameters that differ in the case of the oxidation or reduction [82].

The comparison between the kinetic electrical characterizations (straight lines) with the fit obtained by the variation of the areas underneath the reflectance spectra (dotted lines) is reported in Figure 3.6.

Comparing the electrical behaviour of the sample with trends obtained from the fit of the reflectance measurements, we can conclude that the two different methods provided rather similar results in term of informations deducible from the curves: the saturation times and the variation rate of the curves obtained from the reflectance spectra are in good agreement with the classical electrical measurements.

This means that all the informations deductible form the kinetic electrical characterization such as the time response and the conductivity level of the

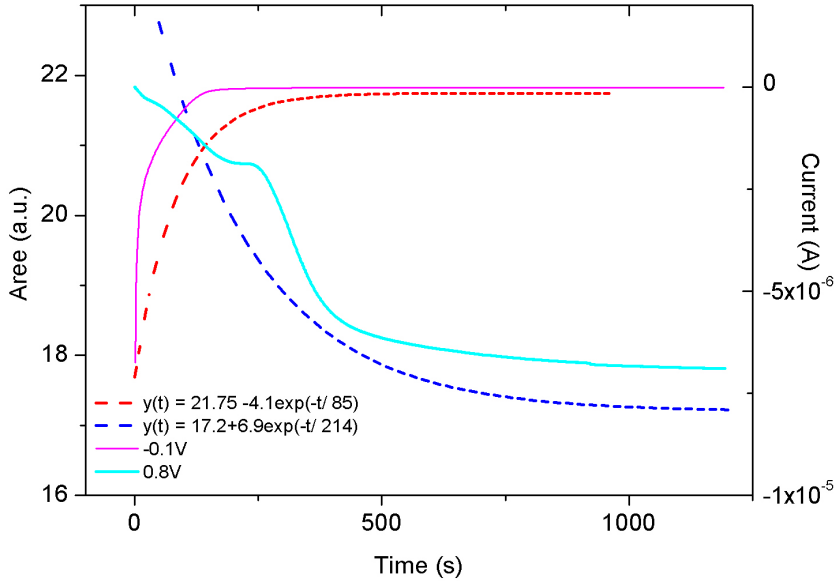

Figure 3.6: *Comparison of optical and electrical measurements during the process of depression (red and pink curves) and of the potentiation (blue and light blue curves) of the conductivity of the organic memristive device: dotted line curve for the area's fit and straight lines for the current variation. The sign of the current and the fit of the areas in the potentiation curves were inverted.*

device, can be extracted also from the reflectance spectra. The great potentiality of this new approach has to be seen in the perspective of a bigger and more complex network of devices in which the necessity of acquiring conductivity informations of the single unit has to match the requirements of a fast answer that does not perturb the system connections. Since, as said before, the spectrophotometric analysis requires 1 min for scanning an area of up to half a meter, this method can acquire informations of different devices in the same time not disturbing or perturbing the state of the devices or the devices directly connected in the network [82].

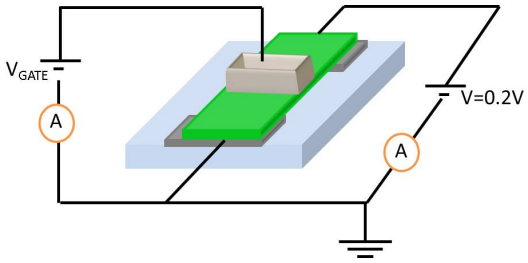

Figure 3.7: *Memristor in transistor mode regime: scheme of the device and set up of the experiment [83].*

3.1.2 Memristors in transistor operational mode

Recently we exploited the possibility of driving an organic memristive device as a transistor, taking advantage of the common electrodes structure between the two types of devices [83]. The devices preparation was performed as reported in [74] in which instead of using the standard polyeletrolyte preparation (a water solution, 20 mg/ml ,of polyethylene oxide (Mw= of $8'10^6$Da) , doped with 0.1 M $LiClO_4$) we used a polyelectrolyte that results from its dilution in water (with a ratio of 1:2). A shown in Figure 3.7, it was necessary to apply a small well of poly(ethylene-vinyl acetate) in the center of the sample to contain the liquid polyeletrolyte solution. As in the standard device, a reference electrode made of a silver wire (diam. of 50 µm) was surrounded by the PEO solution and in this specific case this latter was not just grounded but was connected to one of the SMU unit of our electrical measurement set up (NI PXle-4138). The circuit of the source and drain electrode was closed in the other Source Measure Units (NI PXle-4139). As usual, to ensure the correct estimation of the currents and the proper voltage distribution in the PANI channel, the two grounds of the two circuits (gate and source and drain) shared the same ground potential (Figure 3.7).

For our measurements we decided to apply the fixed voltage value of 0.2 V between S and D electrodes and to modulate the gate voltage varying its potential in the range -0.4 V ÷ 0.4 V starting from 0 V and following a triangular

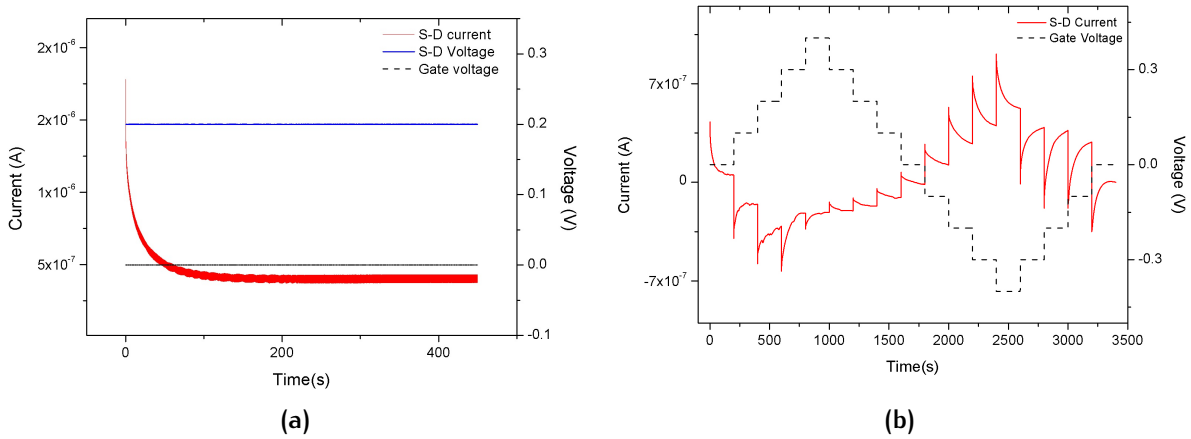

Figure 3.8: *Time response of the output current (I_{SD}) of the device (straight red line) as a function of the gate voltage modulation : a) no gate modulation is applied (black line) while in b) the gate modulation is in the dotted black line[83].*

shape with steps of 0.1 V each 200 s; the voltage value between the source and drain electrodes ensures the possibility of reading the total current of the device without concurring at possible conductivity variation of the polymer. The profile of the gate voltage and the resulting output current, acquired with a sampling period of 250 ms, are reported in Figure 3.8.

In absence of gate modulation, i.e. where the gate voltage is constantly zero (Figure 3.8 a)), the current output of the device (red curve), after an initial transient period due to the parasitic capacitances, reaches a constant value due to the application of the voltage between source and drain (blue curve). Instead, in Figure 3.8 b) where the gate voltage follows the trend previously described (black dotted curve) and the source and drain voltage is kept to the value of 0.2V, the profile of the current doesn't reach a constant value and its behaviour is modulated by the variations in the gate voltages (as expected in a transistor operational mode [84]).

As already explained, the application of a fixed voltage between S and D electrodes induces a distribution of the potential along the PANI channel that results in a potential of the half of the original applied value in the centre of

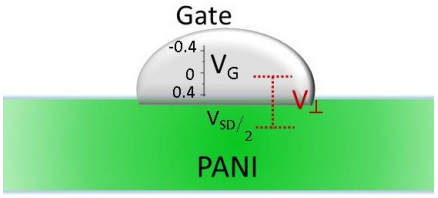

Figure 3.9: *Scheme of the voltage distribution.*

$$V_\perp = \frac{V_{SD}}{2} - V_{Gate} \quad (3.2)$$

the active zone. If the gate potential is kept grounded, this originates a voltage distribution across the interface between the PANI and the polyelectrolyte , that feels a ground potential in one side and a positive or negative voltage at the others [75] (Figure 3.9). A simple mathematical representation of this effect can be written in the equation 3.2, where $V_\perp$ is the voltage distribution across the interface, $\frac{V_{SD}}{2}$ is the half of the potential applied between source and drain (constant in our experiment) and V_{Gate} is the gate potential.

The variation of this latter parameter induces a consequent variation of the potential distribution at the interface between PANI and the polyeletrolyte following the Equ. 3.2. In fact, in case reported in Figure 3.8 a), V_{Gate} is zero and $V_\perp = \frac{V_{SD}}{2}$ and, as expected, the application of such constant voltage induces a constant current output from the device; in this configuration to induce a reaction in the polyaniline layer V_{SD} must be higher than 0.6V or lower -0.1V [75].

Instead in the case reported in Figure 3.8 b), the variation of the V_{Gate} leads to the consequent increase or decrease of the value of $V_\perp$ that affects the total current of the device with its changing. Plotting the time response of the output current together with the $V_\perp$ profile (Figure 3.10), the two curves have exactly the same trend, confirming the effectiveness of the simple model we have proposed and the possibility of driving an organic memristive device as a transistor.

Moreover we can make some further observations: in Figure 3.10 in the time interval between $600 \div 800$s the application of 0.3 V at the gate voltage leads to

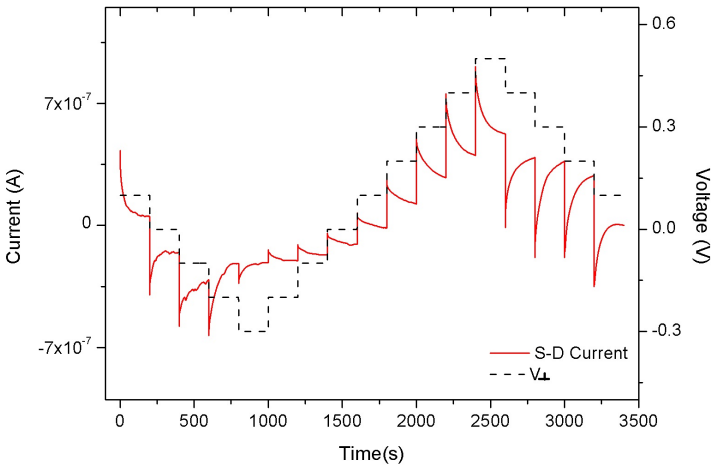

Figure 3.10: *Time response of the output current (I_{SD}) of the device (straight line) and $V_{\perp}$ voltage (dotted line) [83].*

the effective potential of $V_{\perp}$= -0.2V; in the same period the SD current presents a strong decrease of its value, even if both the gate and the SD potentials are positive. This effect can be explained just considering the sum of voltage distribution of Equ. 3.2 according to which the total potential that the active zone feels is negative and so prone to induce the partial reduction process of the PANI channel.

As confirmation of the previous point, comparing the 3 steps ($0 \div 200s, 1600 \div 1800s, 3200 \div 3400s$) in which we applied $V_{Gate} = 0V$ ($V_{\perp}$= 0.1V) we can underline a decrement of the current before and after the reduction process, while it remained practically constant after that.

In this sense, we demonstrated that memristors are able to mimic the transistor operation mode, varying the output current in response to a temporary variation in the gate applied potential; moreover if they are used in a working voltage range in which the voltage distribution across the interface is prone to reduce or oxidate the polymer (according to a sufficient application time) , they can undergo redox reversible reactions that induce stable variations in the conductivity properties of the PANI and consequently of the device. This point is

the main difference between the memristor in transistor mode and the organic transistors that presents a temporary current behaviour in response of a gate modulation, meaning that once that the gate potential is removed, the current naturally return to the previous value at gate potential zero. What we have just demonstrated is that if the $V_{\perp}$ applied to the memristor remains in certain parameters, the current is modulated by the gate potential but if it overcomes certain threshold, the current results from the superimposition of two effect: a stable current mastered by the redox reaction of the PANI and a variable current modulated by the gate variation in the gate potential. This leads to the creation of a hybrid device that presents typical features of the transistor but also typical features of the memristor such as the creation of internal memory states.

Moreover, we decided to test the ability of a memristor to operate in transistor mode even in the case of a gate modulation with pulses with a neural-like spike shape: starting from the bias voltage of 0V, we increased the potential with steps of 0.08 V until the reaching of 0.4V and then we rapidly decrease it until the value of -0.4V. From -0.4V we increase the potential coming back to 0V with steps of 0.08 V. Every step of potential has a duration of 5 ms and so the total spike had a duration of 70 ms.

Results, shown in Figure 3.11, demonstrate that the organic memristive device is able to detect small and fast oscillation of the V_{Gate} voltage inducing a variation in the I_{SD} current of 200% , even if the modulation is of small intensity ($\pm 80mV$) or of a short duration (5 ms). This latter result paves the way for an interesting and ambitious application of memristors as devices for the revelation and acquisition of the neuronal firing signals [83].

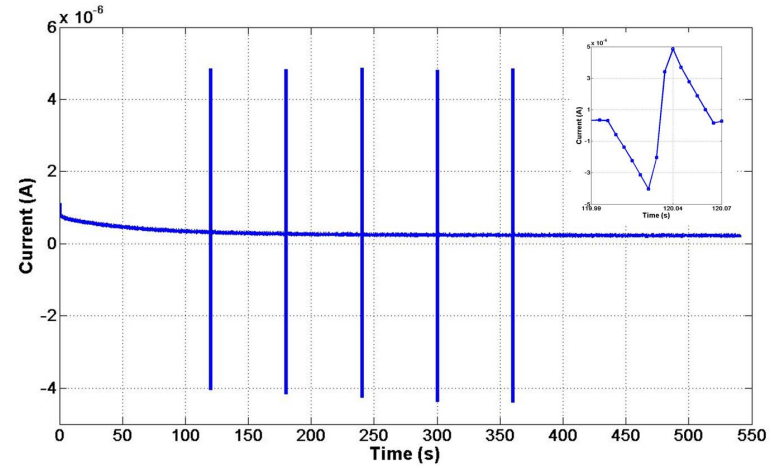

(a) I_{SD}

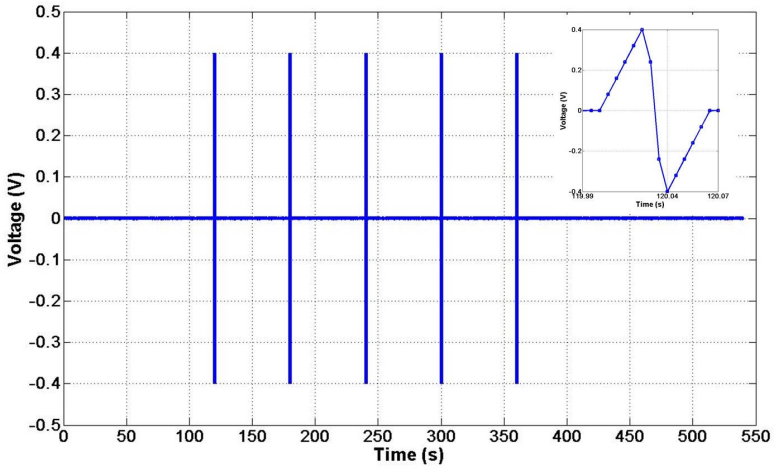

(b) V_{Gate}

Figure 3.11: *Time response of the output current (I_{SD}) of the device and V_{Gate} voltage; in the insets are shown two magnifications of the respective curves [83].*

3.1.3 LTP and LTD: threshold and frequency response

In order to verify the possibility of implementing homosynaptic plasticity features, we realized memristive devices with the same method proposed in [74] and we connected the two circuits (gate and source-drain circuit) to the Source Measure Units NI PXIe-4138/9 equipment. The currents from both the circuits were acquired but, as usual, the potential was applied only between the S and D electrodes while the gate remains as reference electrode to the ground.

The two types of the homosynaptic plasticity that mainly affect the capacity of the brain to memorize, are the Long Term Potentiation (LTP) and Depression (LTD) [54]. Repeated stimuli in a specific synaptic site are able to induce the potentiation or the depression of the synapse depending on the characteristic of such kind of solicitation that the cells received. In fact, each neuron in the brain is highly connected with other neurons and a postsynaptic neuron receives and sums various presynaptic inputs and this summation, also known as synaptic integration, is temporarily and spatially correlated and can be either linear or nonlinear [85]. Although synaptic behaviour has been imitated by hardware-based neural networks, the memorizing ability can be hardware implemented using a memristive or a resistive switching device, taking advantage of their already mentioned memory properties [54].

Thus we decided to implement both the LTP and the LTD neuromorphic functions applying two different voltage pulses to the devices:for the potentiation, stimuli had an amplitude of 0.8V and a duration of 10 ms and two subsequent pulses were separated by 10 ms in which the bias potential of 0.2V was applied; in the case of the depression, the pulses had an amplitude of -0.2V.

Furthermore, we considered the effect of the different number of stimuli, that we consider as our training process, on the output current of the device, thus implementing the temporal integration. Our training routine consisted of

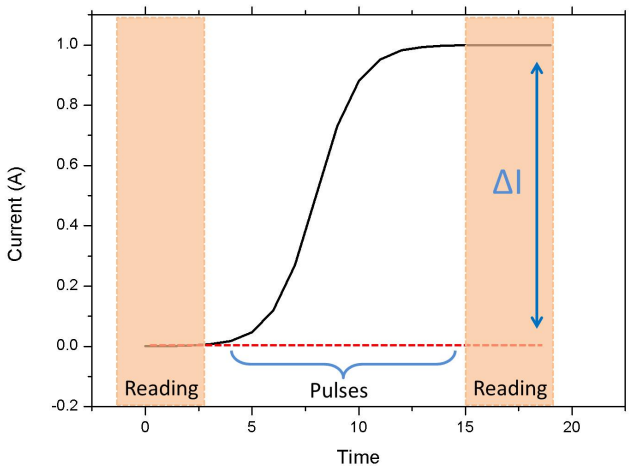

Figure 3.12: *Example of a typical current output: after an initially reading phase of 1 minute, the system was stimulated by the application of voltage pulses that are followed by the conclusive reading phase. ΔI is the difference between the current obtained in the first and the last reading phases.*

different steps: 1) potentiation or depression of the conductive properties of the organic memristor with the application of 0.8V or -0.2 V respectively for reset the system from the previous operation; 2) application for 1 minute of a "reading" voltage of 0.3V ; 3) application of N number of spikes working as stimuli and 4) again the application of the reading voltage. The application of reading voltages is necessary for the correct estimation of the variation in the conductivity state of the device and thus we decided to extend these reading steps to 1 minute in order to allow the reaching of a steady state before the acquisition. In Figure 3.12 an example of the typical current output is reported with highlighted the training routine steps.

Initially the memristive system was tested applying consequently 0.8V for 10 minute and -0.2V for 10 minute; results, shown in Figure 3.13, demonstrate that after 600 s of the application of the positive bias, the percentage variation of the current ($\frac{\Delta I}{I}$), calculated considering the difference between the values in the two reading regimes divided by the initial current value, is of 600 % while in the negative case the current variation is of about (86 %).

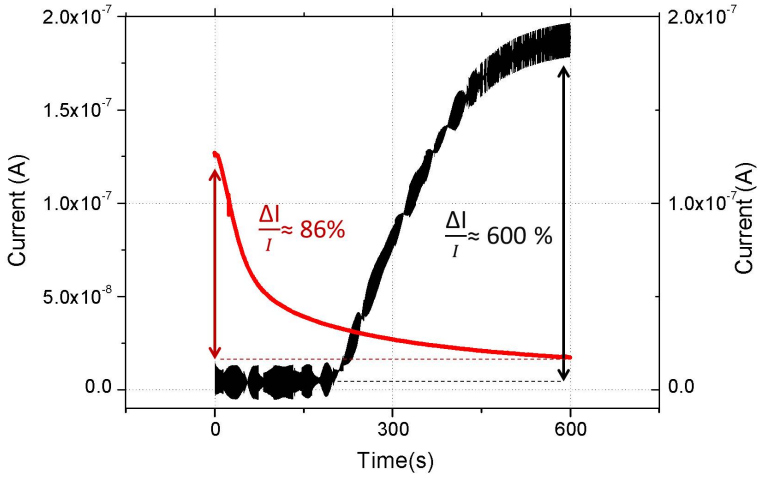

Figure 3.13: *Output current of the device in response to the application of a positive bias (black curve) and a negative one (red curve).*

In Figure 3.14 and Figure 3.15 the obtained percentage variations of the current ($\frac{\Delta I}{I}$) are reported in function of the number of spikes received by the memristor in the case of the LTP and LTD, respectively.

As shown in Figure 3.14, a low number of spikes (< 5k) is not able to induce a significative variation in the conductive state of the device and this results in a small, practically zero, variation in the current before and after the training pulses. This effect was observed also in [85, 54] and classified as Short term potentiation (STP) that is a temporal enhancement of a synaptic connection, which then quickly decays to its initial state. However, increasing the number of pulses, the difference between the two regimes becomes gradually wider till the reaching a total variation of 400 % after 36k stimuli. In this sense, the device exhibits a gradual transition from STP to LTP, similar to biological systems [86, 87, 85].

In the case of the depression of the system (Figure 3.15), the depression counterpart of the STP, the STD, wasn't observed and even in the case of 100 stimuli (2s) the devices produced a variation of 10% that is significative in respect of the variations reported after a bigger number of stimuli. However a progres-

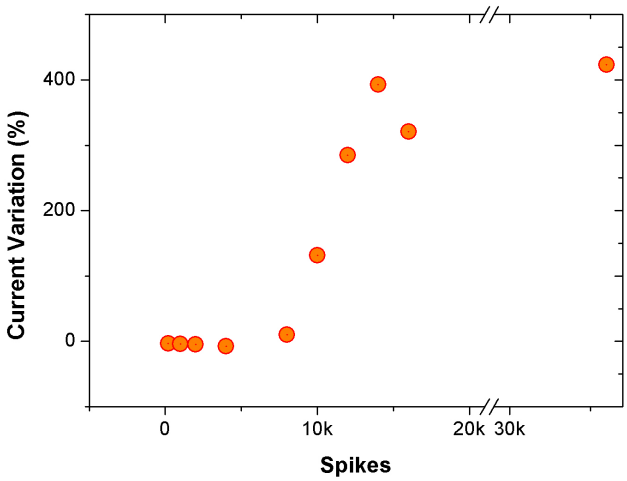

Figure 3.14: *The percentage variation of the current ($\frac{\Delta I}{I}$) versus the number of spikes in the LTP.*

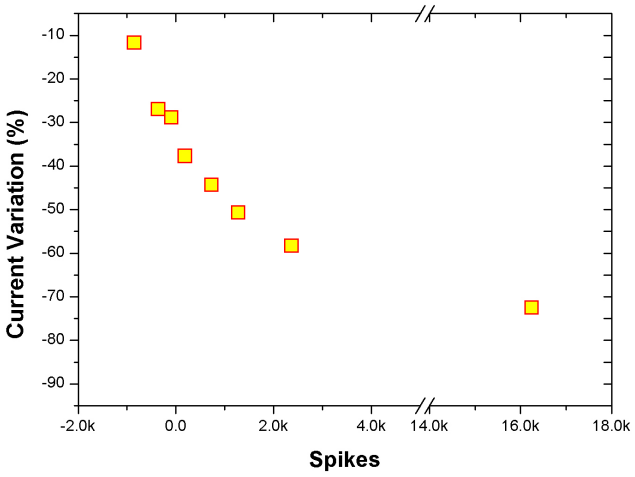

Figure 3.15: *The percentage variation of the current ($\frac{\Delta I}{I}$) versus the number of spikes in the LTD.*

sive reduction of the current can be appreciated in function of the number of applied spikes.

Furthermore we decided to exploit the effect of the frequency of the pulses, varying the application of the bias potential of 0.2V from 10 ms to 110 ms and leaving the pulse duration and amplitude as it is. Results are shown in Figure 3.17 and Figure 3.16 in comparison with the already discussed results and with inset images showing the applied pulses.

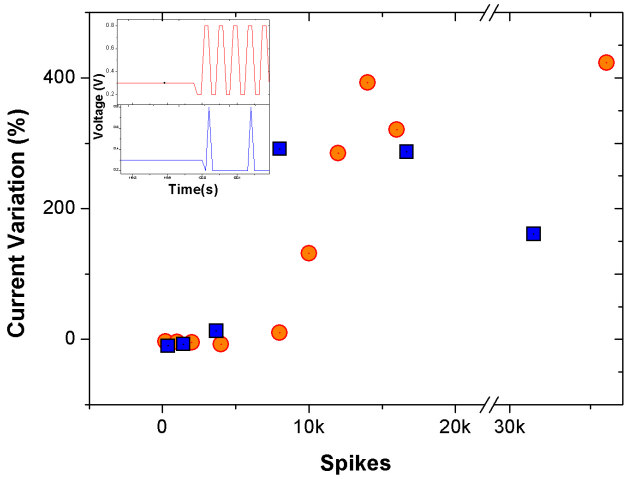

Figure 3.16: *The percentage variation of the current ($\frac{\Delta I}{I}$) versus the number of spikes in the LTP for a higher and a lower frequency stimuli: red circles for the higher frequency and blu squares for the lower. In the inset the two pulses profiles.*

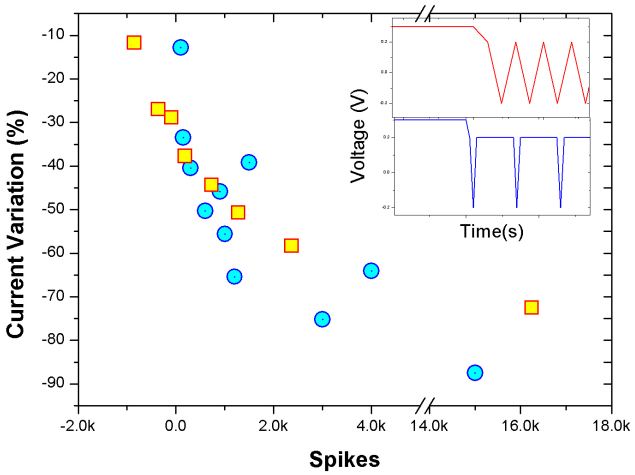

Figure 3.17: *The percentage variation of the current ($\frac{\Delta I}{I}$) versus the number of spikes in the LTD for a higher and a lower frequency stimuli: yellow squares for the higher frequency and blu circles for the lower. In the inset the two pulses profile.*

Results reported in Figure 3.16 show that the variation of the pulses' frequency seams to have no effect on the general trend of the current percentage variation and in fact, as in the previous case, after a low number of stimuli the system presents small perturbations that became significative with the increasing of the number of spikes. However, in relation with the result obtained with a higher frequency, in the range between 5K and 10k spikes, the system presents

an initially wider variation that then remains stable and does not reaches the maximum value of 400%. Even in the case shown in Figure 3.17, the reduction of the frequency of the pulses doesn't affect the kinetic of the current variation that remains basically overlapped to the previous results. However, it's to note that with this set of measurements the current variation reached its maximum of −90% afterwards a lower number of stimuli in respect to the previous case.

Since in both experiments (LTP and LTD) the two sets of measurements with difference frequencies are done in sequence, the faster response at the stimuli observed in Figure 3.16 and the more efficacy of the stimuli reported in Figure 3.17 can be attributed to the memory property of the organic memristive device that once trained, is able to respond faster and better to repetitive inputs [75].

However, even if the method that we have reported for the implementation of LTP and LTD neuromorphic functions is already accepted and used by different groups working in the neuromorphic environment [85, 54], this latter as it's setted, doesn't include the shift from LTD to LTP in response of a frequency variation of the stimuli. More in detail, in a synapse few seconds of tetanic stimulation (high-frequency sequence of individual pulses) enhance the synaptic strength while long periods of low frequency stimulation induce the depression of the connection [33].

For this purpose, we decided to test our memristive devices applying the same pulse in term of amplitude and duration for both the potentiation and depression cases but varying the frequency of the spikes. This approach is rather constraining since in other papers [56] the variation of the frequency was applied to pulses that differ in the case of LTP or LTD by the polarity. For this experiment we used a spikes with 500 ms of duration and 0.8V of amplitude superimposed to the bias voltage of -0.1V . The variation of the frequency consists in the variation of the time between two consequent spikes

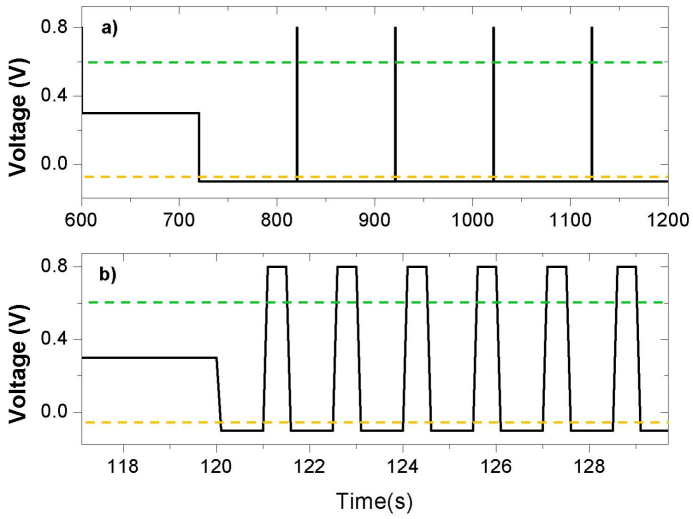

Figure 3.18: *Voltage profile of the pulse used for the implementation of the frequency dependent transition between the LTD (panel a)) and LTP (panel b)) regime. Dotted lines highlight the oxidation (green) and reduction (yellow) threshold voltages.*

and in the case of the potentiation this parameter is setted to 1s while in the depression it's shifted to 100 s (Figure 3.18).

In Figure 3.19, the final profiles of the voltage are reported for both the depression (panel a)) and potentiation (panel b)). In the first case, two reading steps, in which the voltage is setted at 0.3V, are separated by the stimuli application in which the voltage follows the already described pulse form (Figure 3.19 a)). In Figure 3.19 b), instead, the voltage profile presents different reading phases (6 in total) alternated to 5 stimuli periods in which the voltage pulses are separated by 1 s each.

The device output currents, reported in Figure 3.20, show that in the case of the higher frequency stimuli (black curve) the current tends to increase with the application of sets of spikes while in the case of the depression process (blue curve) the current has a abrupt decrease after the first set of applied pulses. This preliminary result is confirmed by the analysis of the current measured in the reading phases between set of pulses, reported in Table 3.1 : in the case of high frequency stimuli the memristive device increases its conductivity while in the case of a lower rate the resistance of the device increases rapidly.

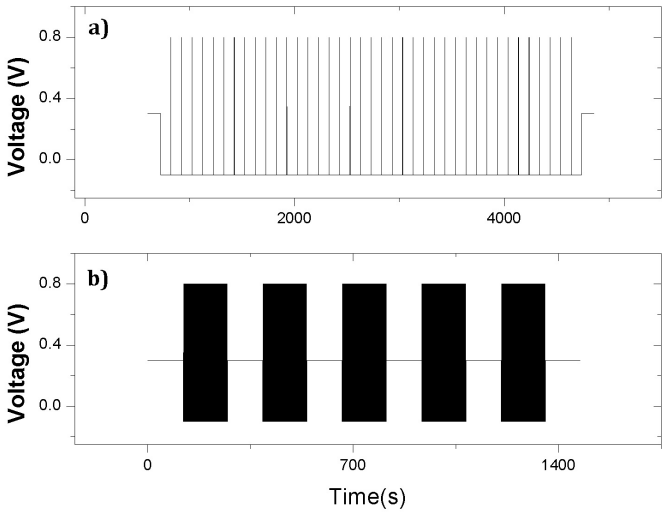

Figure 3.19: *Final voltage profiles for the depression (panel a)) and potentiation (panel b)) experiment.*

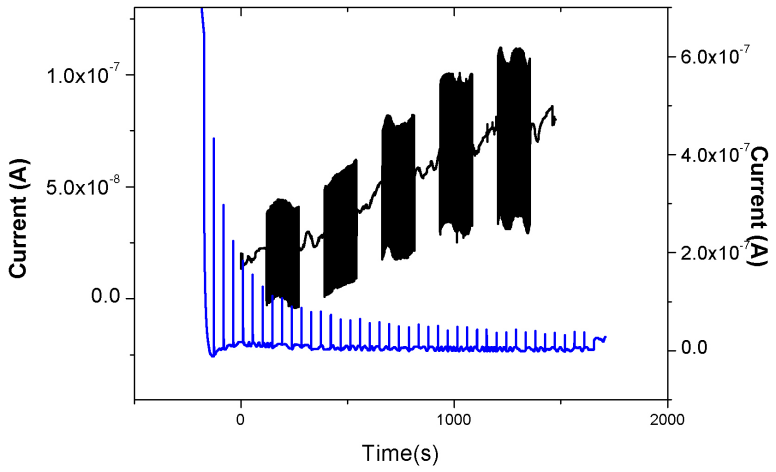

Figure 3.20: *Device output current in the potentiation regime (black curve) and in depression regime (blu line).*

This result on the one hand is in a good agreement with the biological synaptic behaviour and on other hand, is a further demonstration of the tuning facility of the organic memristive devices that can be effectively programmed for answer following specific needs.

Concluding, we demonstrated that organic memristive devices can reproduce neuromorphic functions, exhibiting temporary and/or non-volatile variation of the drain current in function of the number of the stimuli that receive,

N	LTP $I(A)x10^{-6}$	LTD $I(A)x10^{-6}$
1	2.1	6.46
2	2.4	2.33x10-2
3	2.45	-
4	4.01	-
5	4.6	-
6	4.95	-

Table 3.1: *Current values measured in the reading phases between set of pulses.*

in analogy with biological memory. The device can operate in the potentiation case either in its STP or LTP regime, depending on the intensity of the training scheme, and in depression mode, can operate in LTD. Moreover we further extended this concept, exploring the real and most critical parameter that distinguish the LTD from the LTP process: the time frequency of the stimuli. We successfully tested our organic memristors using the restriction of varying their output current just in term of the frequency of the pulse but leaving unchanged the pulse shape.

3.1.4 Simple circuit for heterosynaptic plasticity

In order to implement the heterosynaptic plasticity with organic memristors, it was necessary to realize a different device's geometry basically for taking into account the different morphology of such kind of synapse. In fact, this latter is formed by a pre- and a post synaptic neuron and a modulatory neuron, the function of which is exactly the modulation of the properties of the other channel through its facilitation or activation.

In other words, if the modulatory neuron does something, the channel formed by the pre and postneuron has to be modified.

The geometry we decided to implement is reported in Figure 3.21 a) and it differs from the standard one by the addition of a second PANI channel and

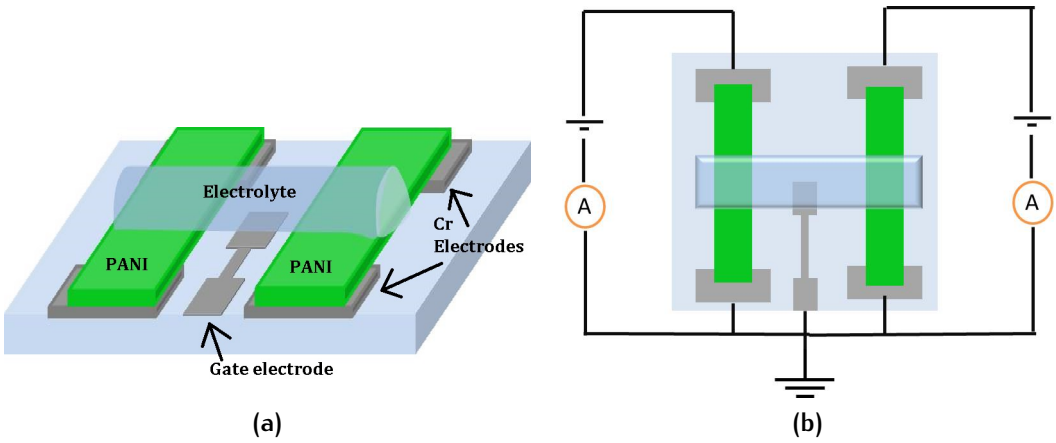

Figure 3.21: *Heterosynaptic plasticity: scheme (a)) and connection diagram (b)) of the device [88].*

a common polyeletrolyte layer that bridges the two conductive channels. The composition and the preparation of the electrolyte is the same used in our standard device and in order to ensure the correct potential distribution in the devices, it's kept at the ground potential by the gate electrode [88]. The conductivity variations of the two PANI channels are acquired separately using the already mentioned Source Measure Units NI PXIe-4138/9 and the dedicated Labview codes and the diagram of the connection is reported in Figure 3.21 b). One of the PANI channels represents the pre and post synaptic channel and so it has just a reading function meaning that we want to read any variation of its conductivity in response of the stimuli received by the other PANI channel, that instead has a modulatory action. For this reason we applied to the first channel the constant potential of 0.3 V that ensures the possibility of reading the current variations but in the same time that the polymer will not undergo to any redox reaction; while to the second modulatory channel we varied the potential. In the first test this second potential followed the curve reported in the bottom part of Figure 3.22 so it started with -0.1V and after 500 s it reaches the value of -0.7V and we acquired the current output of the first PANI channel (upper part of Figure 3.22).

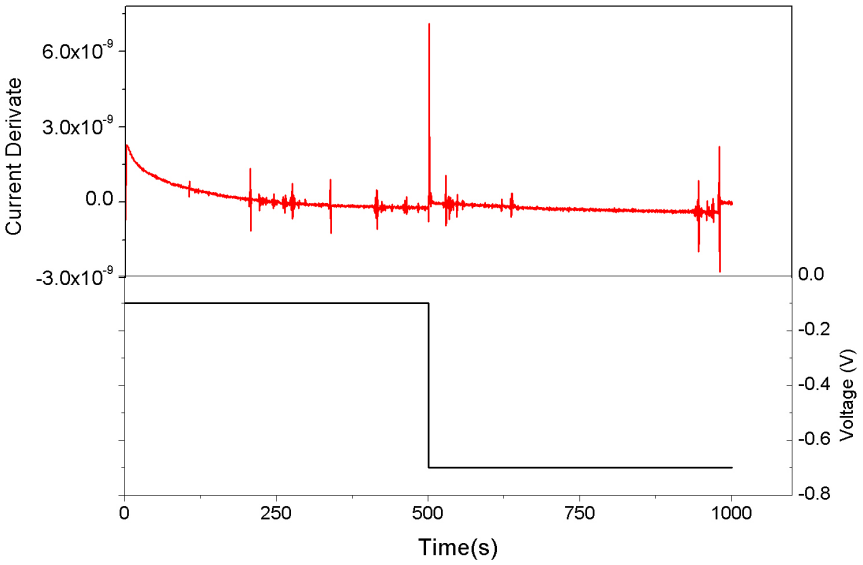

Figure 3.22: *Current output derivative of the first PANI channel (red curve) in response of the variation of the second PANI channel voltage (black curve)[88]*

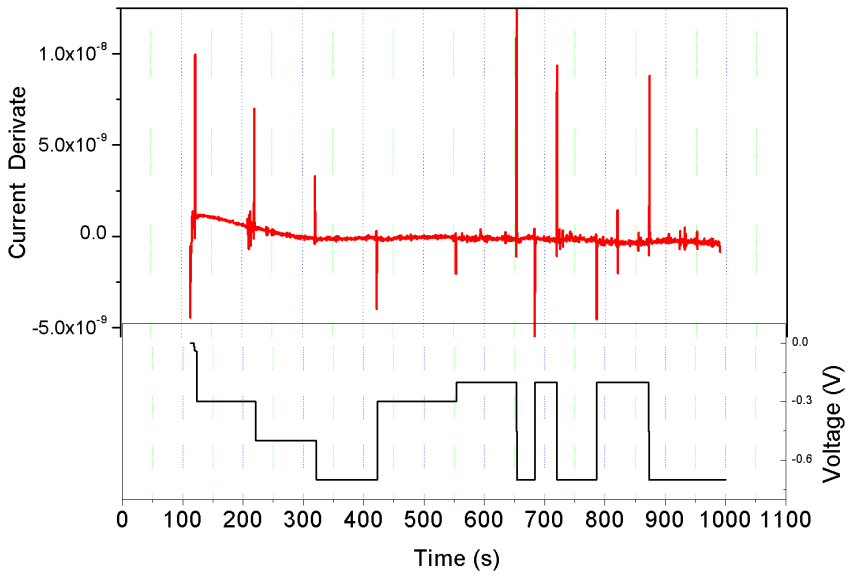

Figure 3.23: *Current output derivative of the first PANI channel (red curve) in response of the variation of the second PANI channel voltage (black curve)[88]*

In order to underline the effect of this step of the potential, from the output current profile it has been removed the baseline curve and then it was performed the derivative of the resulting curve. As it's clear from Figure 3.22 in correspondence of 500 s the derivative curve presents a big peak that stands out in respect to the others due to the noise of the electrical measurement. This effect is further demonstrated by the results shown in Figure 3.23 where even if the modulation of the second channel potential presents a strong heterogeneity from both voltage amplitude and application time (black curve), the first channel current output follows them correctly (red curve).

Furthermore, we exploited also the effect of the variation of the amplitude (Figure 3.24 a), b) and c)) and of the application time (Figure 3.24 d), e) and f)) of the second PANI layer voltage (black curves) to the output current of the other channel (red curves) and as shown in the respective images, it's possible to distinguish in the output current the response due to the voltage variations respect to the spikes resulting from the electrical noise. Moreover the derivatives of the output currents in Figure 3.24 present a partially dependency over the amplitude of the modulation voltage: spikes are less intense in the case with a variation up to -0.3V (Figure 3.24 a)) and their intensity increases with the increasing of the applied negative voltage (Figure 3.24 b) and c)); this dependency is totally in agreement with what reported in [59] where an increase of the modulatory stimuli induced an increase of the current in the pre and post synaptic channel.

Up to now, we have demonstrated that the current of the first channel of PANI is affected by the variations of the voltage of the second channel and the result of these modulations is clearly distinguishable from the electrical noise, even if the pulses are fast and with lower amplitude. However to demonstrate the heterosynaptic features we have to demonstrate further that the modulations of the voltage induce also an increasing or decreasing of the conductivity

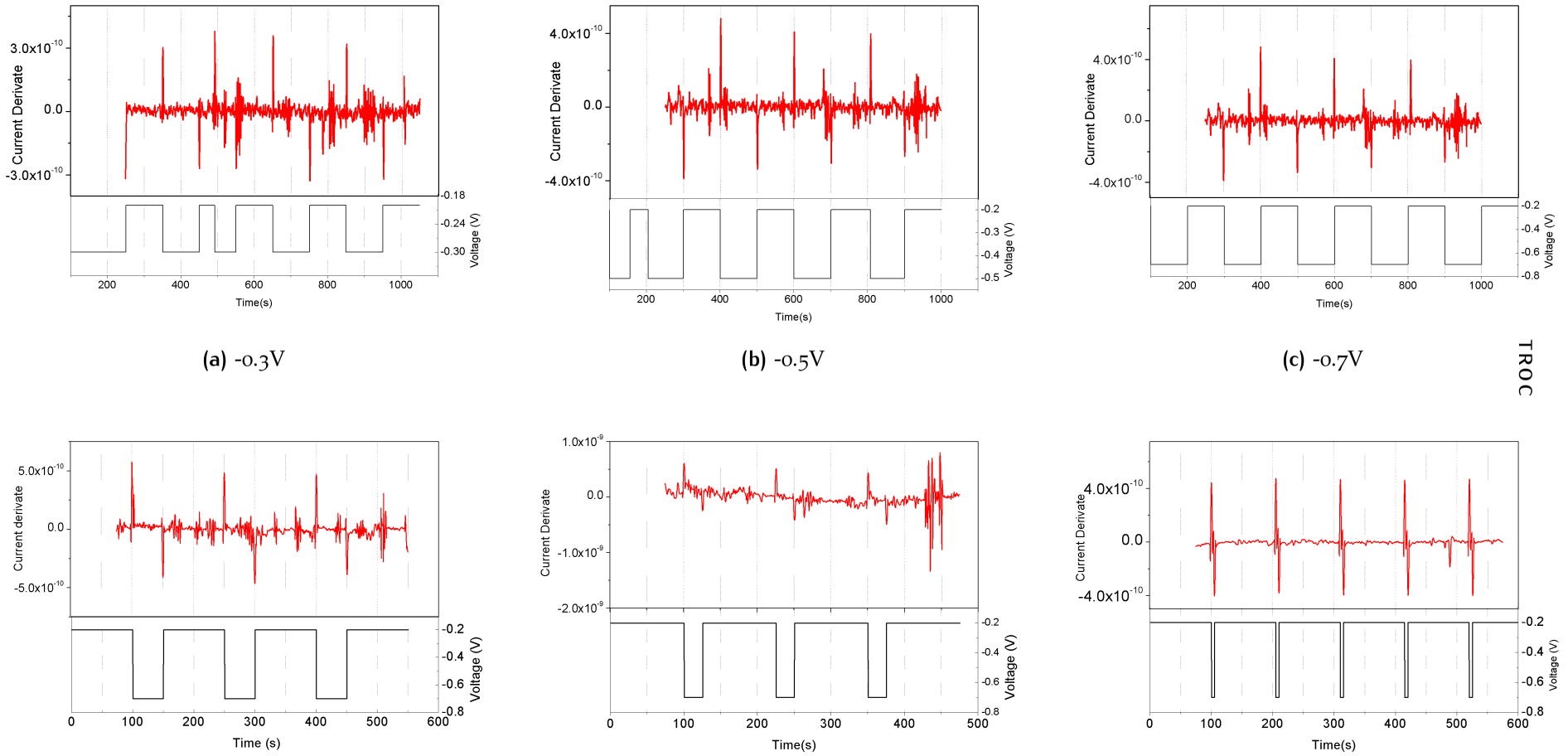

(a) -0.3V **(b)** -0.5V **(c)** -0.7V

(d) 50s **(e)** 25s **(f)** 5s

Figure 3.24: *Current output derivative of the first PANI channel (red curve) in response of the variation of the second PANI channel voltage and application time (black curve): amplitude variations of a) -0.3V , b) -0.5V and c)-0.7V and time application of c) 50s, d) 25s and e) 5s were tested [88].*

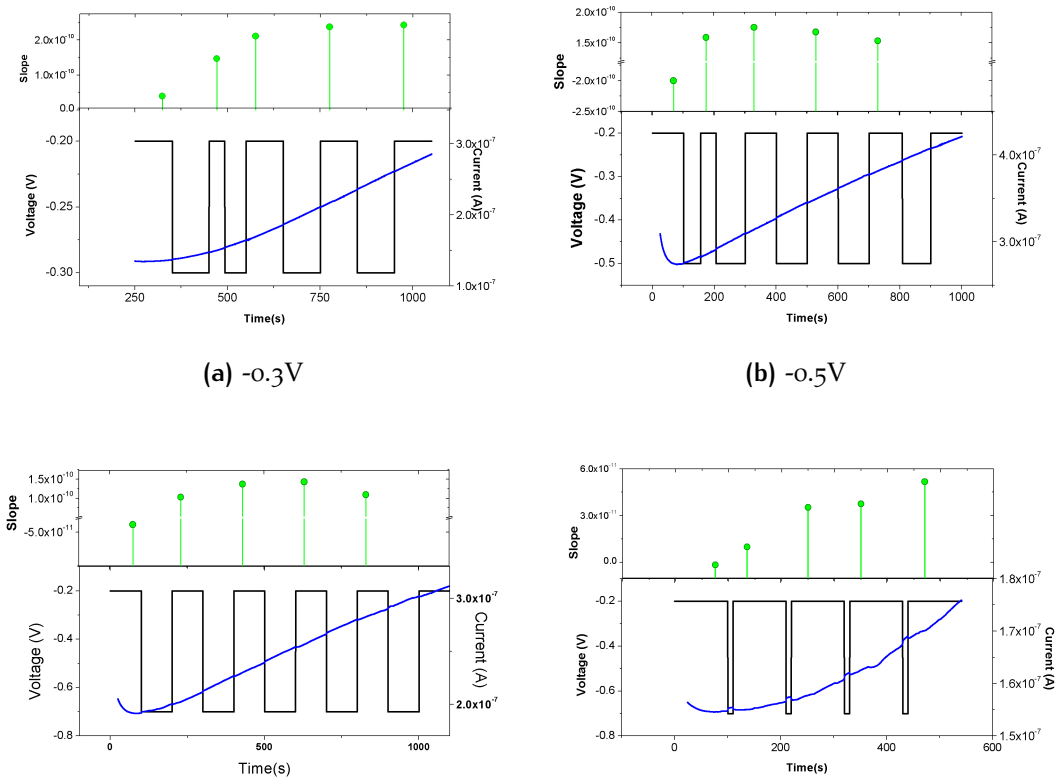

(a) -0.3V

(b) -0.5V

(c) -0.7V

(d) -0.7V

Figure 3.25: *Current output of the first PANI channel (blue curve) in response of the variation of the second PANI channel voltage (black curve). Top panel) time dependency of the slope of the current. We tested the modulation effect for different voltage amplitude(panel a) -0.3V, b) -0.5 V and c) -0.7V) and different application time (panel c) -0.7V for 100s and d) for 5 s) [88].*

of the first PANI layer. In order to do that we plotted in Figure 3.25 the currents of the first channel (blue curve) and the modulatory voltages (black curve) versus the time and we reported in the top part of the graphs also the slopes of the currents, obtained from the linear fitting of the curves, versus the time (green spots). In Figure 3.25 are reported the curves' profile of the performed experiments in the case of -0.3V (Figure 3.25 a)), -0.5V (Figure 3.25 b)), -0.7V for 100s(Figure 3.25 c)) and -0.7V for 5 s (Figure 3.25 d)).

From Figure 3.25 the potentiation effect of the pulses can be appreciated both from the slope variation, that increases in time, and from the trend of the current curves that start to increase when the voltage's steps are applied. Moreover, this potentiation effect is further demonstrated in Figure 3.25 d) where, even if the application of the pulse is reduced to 5s, the increasing of the current is still present but with a more gradually slope variation. This feature can be interpretated taking in consideration the effect of the reduced time in the oxidation or reduction process of the PANI in our memristive device where for switching on and off the conductivity is equally important the selection of the proper voltage values and of the application time.

This observation confirms once more that, in the geometry that we have proposed, any modulations of the voltage, in terms of voltage amplitude or application time, that is applied to one channel affects the properties of the other channel, that responds with a variation in the current. In this sense we can speak about heterosynaptic plasticity.

3.1.5 Fist step: the single-layer perceptron

The ability of memristor to emulate the synapse behavior paved the way for the realization of the first elementary single-layer perceptron fabricated from polyaniline-based memristive devices [89].

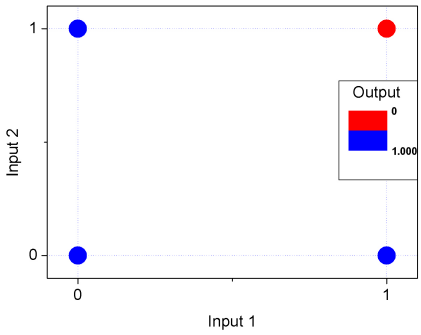

Figure 3.26: *Scheme of inputs and output of the NAND logic function.*

Input	Input 2	Output
1	1	0
1	0	1
0	1	1
0	0	1

Table 3.2: *Truth table of the NAND logic function.*

As mentioned in the section 1.5.4, a perceptron is able to separate input data in different classes and, even in the simplest case (elementary perceptron), is able to classify variables in two linearly separable classes. By definition, two set of data are linearly separable if exists one line able to completely separate one class from the other; an example of this is the logic NAND function, the truth table of which is reported in Table 3.2 and Figure 3.26.

In this specific case, we wanted to train a perceptron to separate the inputs depending on the output that result from a specific function. More in detail, we decided to use as function the NAND logic function in which inputs are given by combinations of 1 or 0 logic (0-0, 0-1, 1-0, 1-1) and the output can be 0 or 1 as well: only one input combination (1-1) provides 0 as output, while the others provide 1.

For this purpose, 3 standard devices, fabricated with the same procedure previously reported in section 2.1, were connected in the scheme reported in Figure 3.27 to three different voltage inputs (x_i). The current output (y) results from the summation of the three contributions coming from the devices and depends over their conductances by the weights $y(x_i) = \sum w_i x_i$.

Furthermore in our input data (x_0, x_1, x_2), two of them (x_1 and x_2) are variable inputs while x_0 is fixed to the value of 1 logic ; in fact, looking at the formula describing the perceptron, we may need to have negative weights w_i

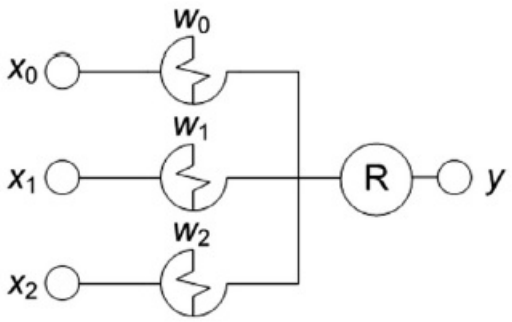

Figure 3.27: *Scheme of an elementary perceptron based on organic memristors [89].*

but since, from a physical point of view, they represent the ratio between the voltage and the current, they cannot be naturally negative and so we need to invert the sign of the voltage of the two variable inputs (x_1 and x_2) respect to the fixed sign of x_0.

In order to perform a logic operation with the elementary perceptron, we need to assign to our input and output physical variables (x_i are voltages and y is a current) the 0 and the 1 logic counterpart values, imposing some "conversion" rules. Taking into account the characterization of a classical memristor, the voltage values in the range between the oxidation and the reduction potentials (0.6 V and -0.1V respectively) do not correspond to any redox reaction in the device active zone and thus ensure the so call "reading" of the conductivity state without any variation. For these reasons we chose |0.2V| and |0.4V| as our 0 and 1 logic input values.

On the other hand, we can define the "writing" potentials as the potentials that induce a modification of the conductivity of the device and in our network we used 0.7 V and -0.2V.

The conversion of the output (y), instead, passes through the comparison between the real current value and a threshold, previously setted and constant for all the learning procedure: if y exceeds this value, it will be classified as 1 and the correspondent input combination will be in the class 1, otherwise it is within the class 0. In our experiment we set a threshold of 3.0 μA and

a demarcation current $\pm$ 0.5 μA necessary to avoid possible misclassification. This classification of the y output using the threshold method directly comes from the activation function, described in the previous chapter, that is part of the perceptron algorithm.

To perform the learning of the classification of the inputs, we decided to use the logic function of NAND and NOR using the algorithm with the error correction suggested by Rosenblatt [89]. In this method, an error function must be defined:

$$e = y - y_t \, , \tag{3.3}$$

where y is the logical output (determined by the threshold method) and y_t is the desired output determined by the truth table of the chosen logic function.

The sign and the value of the e determine if it is necessary to increase or decrease the memristance of the devices and so if it is necessary to induce the oxidation or the reduction of them; in fact if $e < 0$, this means that the desired output is higher than the real output and so the network need to be potentiated for decrease its resistance. To do that it's necessary to apply the writing potential of 0.7 V for a 600 s. In the opposite case, if $e > 0$, the network must be depressed with the application of -0.2V for 30 s (duration of the training was varied: number of necessary training cycles was found to depend on the duration of each training cycle). In the case of a zero error no action is required.

The learning procedure is iterative and it starts with the application of the first combination of inputs to the devices, for example 1,0,0 (0.4V, |0.2V| , |0.2V|) to the network and the acquisition of the current of the system (1.8 μA). Comparing this output with the threshold, it's interpreted as 0 against the desired output that is 1. So in this first case our error value is negative and this means that we need to potentiate the network. Once that we perform this latter step, we can skip to the next input combination and repeating the procedure. The

N	Input			Output	Logic Output	Desired Output	error	Correction time		
	x_0	x_1	x_2	(μA)				0	1	2
1	1	0	0	1.8	0	1	-1	p600	-	-
2	1	0	1	-0.3	0	1	-1	p600	-	d30
3	1	1	0	4.8	1	1	0	-	-	-
4	1	1	1	3.5	1	0	1	d30	p600	p600
5	1	0	0	4.5	1	1	0	-	-	-
6	1	0	1	4.1	1	1	0	-	-	-
7	1	1	0	0	0	1	-1	p600	d30	-
8	1	1	1	3.8	1	0	1	d30	p600	p600
9	1	0	0	5.3	1	1	0	-	-	-
10	1	0	1	5.1	1	1	0	-	-	-
11	1	1	0	0	0	1	-1	p600	d30	-
12	1	1	1	2.5	0	0	0	-	-	-
13	1	0	0	4.6	1	1	0	-	-	-
14	1	0	1	4.5	1	1	0	-	-	-
15	1	1	0	4.0	1	1	0	-	-	-

Table 3.3: *Results of the perceptron learning to perform NAND function [89].*

learning procedure stops when 4 consecutive combinations of inputs result in a zero error. All the steps for the learning of the perceptron are reported in Table 3.3 while in Figure 3.28 the geometrical representation of the perceptron classification is proposed.

Table 3.3 shows that we successfully trained the system to perform the NAND function in 15 steps and after one hour of the learning procedure, this ability remained memorized. After this first test on the NAND function, we tried to re-train the system to perform the NOR function. Surprisingly just 2 potentiation steps were required for the total re-train of the system. In conclusion, we demonstrated to be able to realize an elementary perceptron made entirely by organic memristors the conductivity of which can be varied in order to adjust the actual output of the network to match the desired output value. The elementary perceptron was initially successfully trained to perform the NAND logic function and then consequently re-trained to perform the NOR function. From a geometrical point of view, the perceptron we realized was able to built

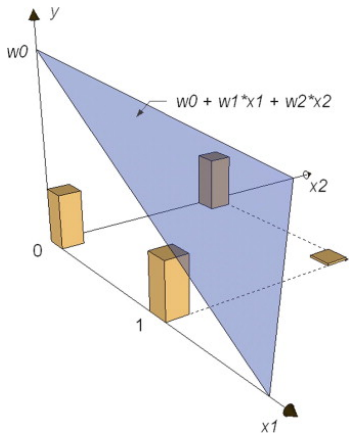

Figure 3.28: *Geometrical representation of the perceptron output (the separating plane) when it has been learned to the NAND function [89].*

the separation plane reported in Figure 3.28 for separating the input combinations in two classes: the ones that result in an output of 1 and the remaining that results in 0.

3.1.6 Next step: the double layer perceptron

The single-layer perceptron is the simplest kind of neural network able to implement basic learning functionalities and parallel processing. However, in the field of artificial intelligence, more complex neural networks are requested to solve demanding tasks for example the performing of linearly nonseparable tasks (i.e. the tasks that cannot be separated by an hyper-plane in the space of their features) cannot be solved by a single-layer perceptron but needs a more complex ANN such as a multilayer perceptron . In this scenario, the main goal of the work presented in this section is the design and the hardware realization of a simple double-layer artificial neuronal network (ANN) based on organic memristive devices that is able to solve linearly nonseparable tasks.

Devices used for that purpose were realized following the procedure and the method reported in section 2.1.1 and the measurement set up used for the application and the acquisition of the output voltages was the NI PXIe-4130,

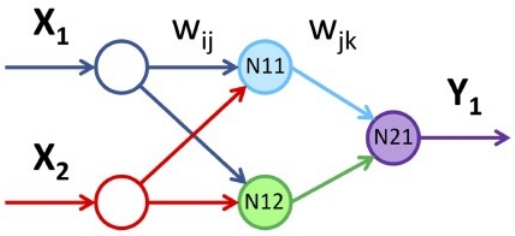

Figure 3.29: *Scheme of a multilayer perceptron: X_i and Y are the inputs and the output of the network while N11,N12 and N21 represent neuron units [90].*

PXIe-4138, PXIe-4139 Source Measure units, NI DAQ board together with two bias voltage suppliers (0.4 and 15 V).

The scheme of the network is reported in Figure 3.29 where two inputs (X_1 and X_2) feed two hidden neurons (N11 and N12 in the scheme) and the outputs coming from these two neurons constitute the input for the last neuron (N21) at the end of which we collect the voltage output (Y_1). The links (W_{ij} and W_{jk}) represent specific synaptic weights between the ith neuron of the first layer and the jth neuron of the second (and so the same for W_{jk}) and in the circuit diagram of the network reported in Figure 3.30, they are represented by the conjunction of two memristors per weights. The simultaneously use in the synapse connection of two memristors ensures the perfect emulation of the biological synapses, where one neuron can be fed up with "excitatory" and "inhibitory" stimuli that must be summed before the neuronal activation. This means that synaptic weights must be equally negative or positive in order to allow the learning algorithm convergence in the selected task [90]. In order to do that, we decided to implement the scheme reported in Figure 3.30 where two memristors play the role of "excitatory" and other two the "inhibitory" one by the connection to non-inverting and inverting inputs of the op-amp accordingly [90]. So if G_i^+ and G_i^- are the the conductances of the i-th excitatory and inhibitory memristive devices respectively, the weight of the i-th synapse

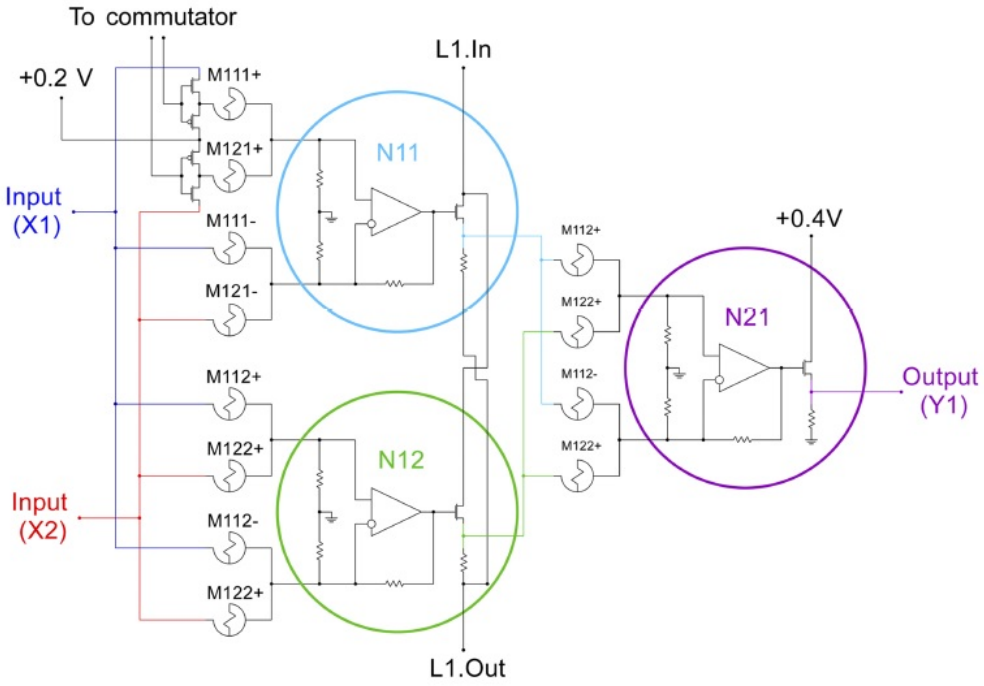

Figure 3.30: *Circuit diagram of the memristor-based ANN:* X_i *and Y are the inputs and the output of the network; the op-amp and the MOSFET enclosed in colored circles represent the neuron units. Memristors are identified by the* $M_{n,i,j}(\pm)$ *codes where n is the index for the layer where the device connected to the i-th input and j-th output neurons; all memristors are connected to an access system that is shown for M111+ and M121+ and omitted for others for simplicity [90].*

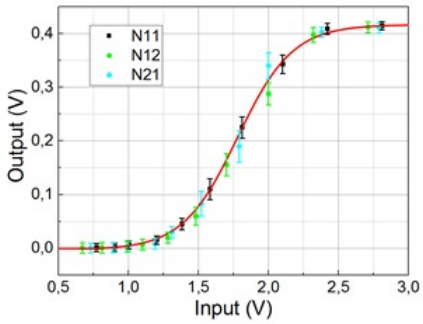

Figure 3.31: *Activation functions of the three voltage dividers implementing an activation function of neurons [90].*

is given by $w_i = R_{fb}(G_i^+ - G_i^-)$ where R_{fb} is the value of the feedback resistance [90].

The op-amps reported in Figure 3.30 constitute the main part of the circuital representation of the neuron units, together with the voltage divider unit realized by means of a MOSFET [90]. This combination is able to provide the basic neuron functions of summation and threshold since the summator performs the weighted sum of the inputs $\Sigma w_i x_i$, the output of which feeds the gate of the MOSFET, dividing the inputs in 1 and 0 logic if the voltage exceeds or not the threshold value that allows the opening of the transistor. In our experiment this threshold was about 1.8V and the typical activation function for our neurons is reported in Figure 3.31 [90].

Moreover in order to correctly perform the training of the network, we developed an access system based on CMOS-transistors that drove the access to every memristive device independently from others and thus allowed the application of writing or reading voltage to the specified memristive device within a training or during information processing. More details about the circuit used can be found in [90].

In analogy with the description given in the section regarding the elementary perceptron's realization, the voltage values of 0.0 V and 0.4V were chosen as reading voltages corresponding to the 0 and 1 logic while for depressing or

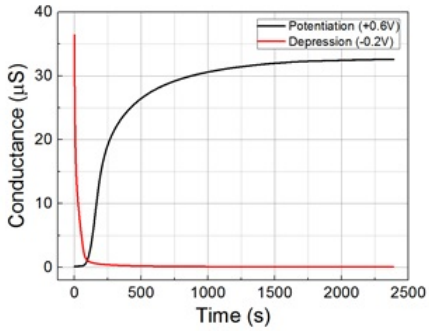

Figure 3.32: *Typical kinetics of the PANI-based memristive device conductance under potentiating voltage (+0.6 V, black line) and depressing one (-0.2 V, red line).*

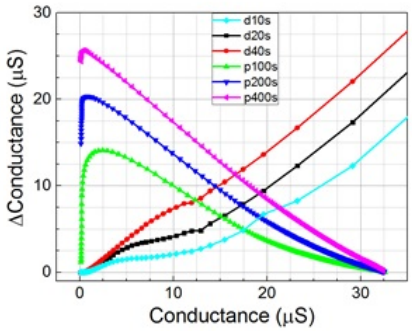

Figure 3.33: *Absolute values of the memristive conductance change under the potentiating voltage pulse (+0.6 V, prefix "p" in the legend) and depressing one (-0.2 V, prefix "d") as a function of the initial conductance, for various pulse durations (specified in the legend).*

potentiating the devices conductivities we used -0.2V and 0.6V respectively. The duration of each training pulses was established considering the typical resistive switching kinetics reported in Figure 3.32 where the time response of the conductance of the devices was plotted. Furthermore we also considered the variation of the conductance (ΔS) plotted versus the initial conductance value for different pulse durations (Figure 3.32).

Since a double-layer perceptron is able to solve linearly nonseparable tasks, we decided to implement a logic non separable function such as the XOR function (Table 3.4) with the ANN that we built.

For the realization of a learning procedure we used a simplified version of the back propagation with batch correction algorithm in which the weight updating is proportional only to the sign and not to the absolute value of weight

Input	Input 2	Output
1	1	0
1	0	1
0	1	1
0	0	0

Table 3.4: *Truth table of the XOR logic function.*

correction defined by the squared error function E [90]. Both the error function and the correction are described in Equ. 3.4 [91]:

$$E = \Sigma_{i,k}(t^k - y^k)^2; \quad \Delta w_{i,j} = \eta \frac{\partial E}{\partial w_{i,j}} \tag{3.4}$$

where t^k and y^k are the expected and the actual output values of the output neuron when a vector of the training set $x^k$is applied. In our case the training set was composed by the four combination of logic inputs (0-0, 0-1, 1-0, 1-1) and the entire procedure was repeated until E=0 . In the standard backpropagation method, this procedure of updating the weights brings to the minimization of the squared error function through a precise tuning of the weight values (sign and absolute value). However in the case of a hardware perceptron, this point has to be faced taking in consideration the unavoidable variability of the real devices. So we managed this issue following the weight correction direction (so the sign), but not its value, choosing the empirically established learning pulse time duration in order to minimize the duration of learning steps, and kept constant (but different for depressing and potentiating pulses) for all steps in the whole learning procedure.

The learning procedure consisted of 3 phases: 1) the application of the training set vectors x^k (30 s per input combination) , 2) actual weight measuring through the application of the "reading" voltages for 30 s and 3) weight correction with "writing" pulses if necessary. This procedure was successfully performed until convergence (E=0) and the output results of the first and after

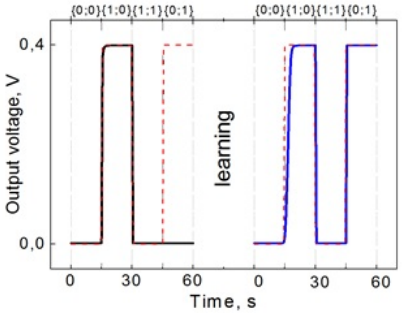

Figure 3.34: Output signal within the epochs before (left) and after (right) training and expected output signal (dotted).

Figure 3.35: Synaptic weights before (black columns) and after (red columns) the training procedure.

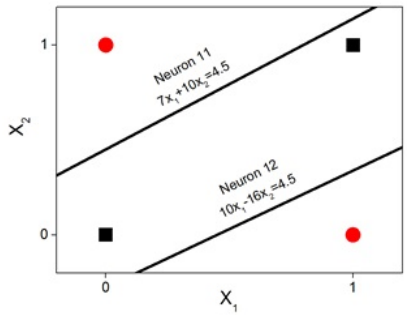

Figure 3.36: 2D representation of the separation in classes performed by the ANN.

the last iterations are reported in Figure 3.34 for XOR logic function, together with the weights variation reported in Figure 3.35.

For the sake of completeness, as shown in Figure 3.34 the first iteration output (back curve) was accidentally rather similar to the desired output (red dotted curve) and this observation is furthermore confirmed by the small differences between the initial and final weights reported in Figure 3.35. However, the simple method that we applied for the training of the network bring to the correct classification of the inputs, separating them in classes by two planes in the feature space (see Figure 3.36 and Figure 3.37)

In conclusion, we have shown that memristive devices can be used in principle for multilayer ANN hardware realization. For the first time, we built a double-layer ANN network that paves the way for the realization of a multilayer perceptron, demonstrating the possibility to perform nonseparable combinational logic classification (XOR logic task). Moreover it's also possible to

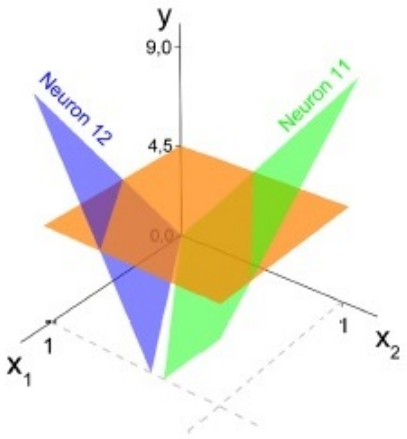

Figure 3.37: *3D representation of the separation in classes performed by the ANN. Area above and below the plane y=4,5 is the class "1" and "0", correspondingly).*

proved that a perceptron principally can solve analogue tasks which cannot be realized by digital devices [90].

3.2 BIOLOGICAL INTERFACES

With the aim of looking at the interface between PANI and different types of cells, we will provide in this chapter, the results of a novel and multidisciplinary study in favour of the PANI biocompatibility. Moreover we will report the realization of a functional interface between a memristive device and living neuronal cells.

3.2.1 Testing the bio-compatibility

The preparation of the PANI substrates was reported in several previous papers [74]: briefly we deposited by means of the Langmuir-Schaefer technique different multilayers of PANI, using the polymeric solution reported in section 2.1.1.

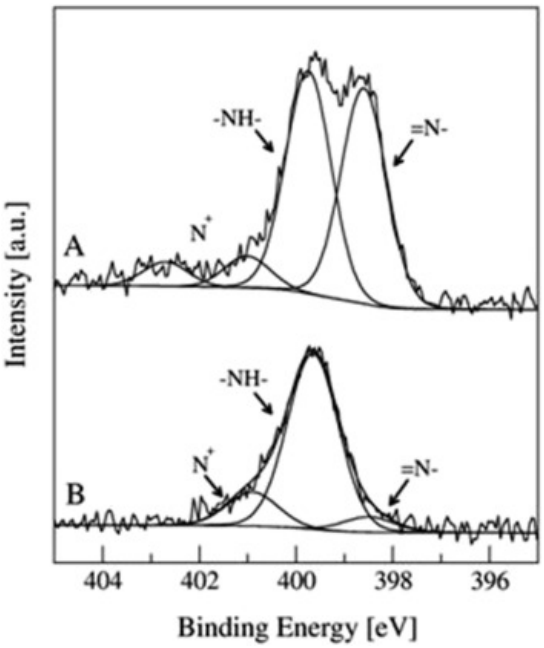

Figure 3.38: *XPS analysis of the nitrogen core lines on PANI emeraldine base films (A) and emeraldine salt (B) [79].*

The number of the deposited layers varies in order to better match the needs of the characterization and the cells culturing steps. In the first case in fact a thicker sample (48 monolayers) is preferable in contrast with the thin sample (25 layers) used in the biological phase. For all the preparations, the substrate used for the depositions was a cover glass insulating support (diam $\approx$ 15 mm). The protonation of the emeraldine base form affects principally the bonding of the nitrogen atoms that pass from a quinonoid imine (=N-) to a benzenoid amine (-NH-) [92]; more in detail, the ratio between these two contributions should pass from 1:1 of the base form to the presence of only benzenoid amine in the salt form ; in fact the performed XPS analysis reported in Figure 3.38 confirm this thesis, showing that samples of the emeraldine base PANI (panel A) present two evident peaks attributable to the two N forms and with ratio between them (0.97) in good agreement with the theoretical value; while in the panel B, samples, resulting after the acid treatments, present an intense peak of the benzenoid structure and a small contribution (9 %) of the quinonoid imine.

Sample	O1s(%)	N1s(%)	C1s(%)	Si2p(%)	Cl2p(%)
Emeraldine base	6.1	11	79.1	3.8	
- Emeraldine salt	11.5	5.7	71.1	9.5	2.2

Table 3.5: *Elemental composition (atomic percentage) of different PANI forms determined by XPS analysis.[79]*

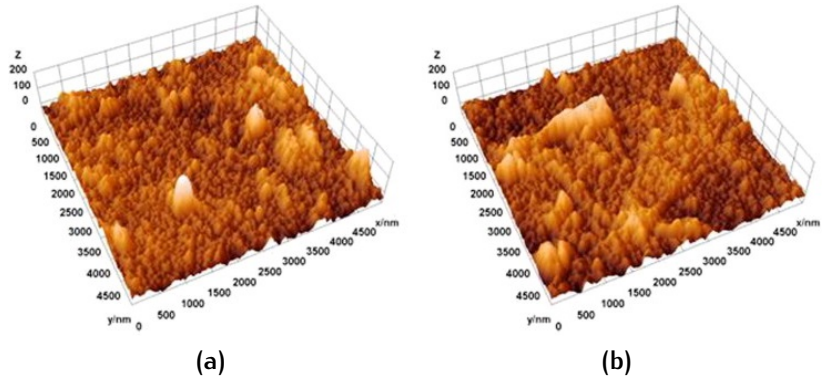

Figure 3.39: *AFM images of different areas of the PANI samples: a) emeraldine base and b) emeraldine salt. Picture taken from [79]*

Moreover, acquiring different core lines gave us the possibility of detecting the presence of some contaminants such as oxygen and silicon elements (shown in Table 3.5) before and after the HCL treatments.

The thickness of the film was estimated to be about 120 ± 13 nm in the case of the emeraldine base form while, after the acid protonation, it slightly decreased to 113 ± 8 nm. This moderate effect (in the order of 5%) was explained in [79] with the possible lost of some polymeric layer during the dipping process; the estimation of the roughness was found to be $25{,}6 \pm 6.0$ nm (emeraldine base) and $27{,}7 \pm 6.3$ nm (emeraldine salt) confirming that PANI films were quite uniform thanks to the chosen deposition technique that guarantees a very good control over the morphology and reproducibility of the samples [93, 94]. The transition due to the protonation seams to not drastically effect the morphology, that doesn't present any major difference between the before and after sample.

To satisfactorily test the biocompatibility of the polymeric layers different cells cultures, human immortalized and tumor cells (HeLa and HEK293T cells) and human neuroblastoma cell line (SH-SY5Y) were prepared following the

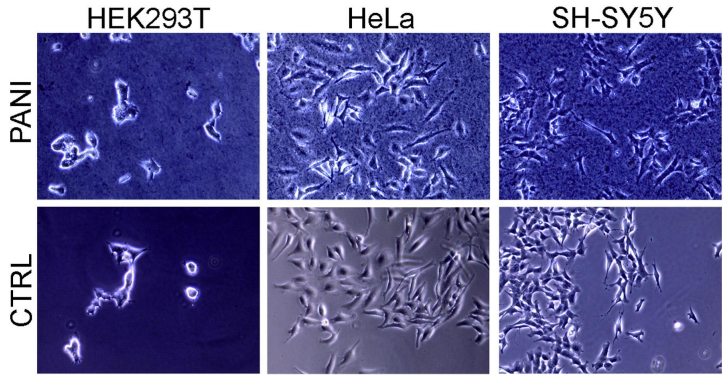

Figure 3.40: *Different cells lines growing on PANI and control samples. Picture taken from [79]*

protocol described in [79] on bare and PANI covered glass slides (Figure 3.40). Briefly, the first two line cells were cultured in DMEM supplemented with 10% (v/v) of fetal bovine serum (FBS), 100 U/ml of penicillin, 100 mg/ml of streptomycin, 2 mM l-glutamine (Lonza) on uncoated cover glass (control samples) and on glass cover of 25 layers of PANI. Samples were maintained at 37 °C with 5% CO_2 at pH 7.4. Human neuroblastoma cell line was cultured for 24 h in complete medium on control and PANI samples. Bright field microscope images reported in Figure 3.40 show the morphology of the different cells lines after 24h on incubation for both the control and the PANI samples.

Comparing the results obtained in term of morphology and number of cells, the growth of the cells seems in all cases quite comparable between the PANI and the relative control samples [79]. Moreover after this first test, the human neuroblastoma cell line was further tested to verify if the presence of the conductive polymer film may affect the differentiation of SH-SY5Y cells towards a neuronal phenotype.

If cultured in normal culturing conditions, this cell line can produce short neurites but they are able to differentiate into a more complex neuronal phenotype if treated with retinoic acid (RA) and brain derived neurotrophic factor (BDNF) following a specific protocol[79, 93]. After the first day after the plating in a complete medium, this latter is changed with DMEM + 15% FBS + 10

μ M all-trans-retinoic acid and kept for 5 days. After that, it was changed with DMEM + 50 ng/ml BDNF.

Images obtained with bright field microscope are reported in Figure 3.41 where the different phases of the differentiation test are reported for both the uncoated control sample (CTRL) and the PANI covered glass (PANI). From these images we can observe the modifications of the cells induced by a different composition of the culturing medium and the end of which the cells have developed neurites physically attached to the surfaces. Once again the appearance of these protrusions suggests that PANI is compatible with the growth and neurites expansion from the cell body that after the treatment, present elongated and arborizated morphology (Figure 3.42) [79].

Concluding, we found out that several cells lines, previously not reported in literature (HEK293, NSC-34 and SH-SY5Y), adhering to poly(anyline) memristive surfaces, are fully viable and show a full and effective capability of growth, proliferation and differentiation even if this unconventional culturing substrate.

3.2.2 Coupling living neuronal cells with organic memristor

The following step was the realization of a functional interface between a memristive device and living neuronal cells. More in detail, the goal of this section is to provide evidences of the possibility of driving organic memristive device not only as an synaptic analogue but also as an artificial synapse. As said before, a synapse is the conjunction between two neuronal cells and thus the work reported here, will describe the result of an experiment, performed in collaboration with the Laboratory of Neurobiology of Kazan Federal University, in which two neuronal cells where connected through an organic memristive device. The cell preparation and the electrophysiological recordings method were reported in [95]; briefly brain slices were prepared from P5–P6 Wistar rats

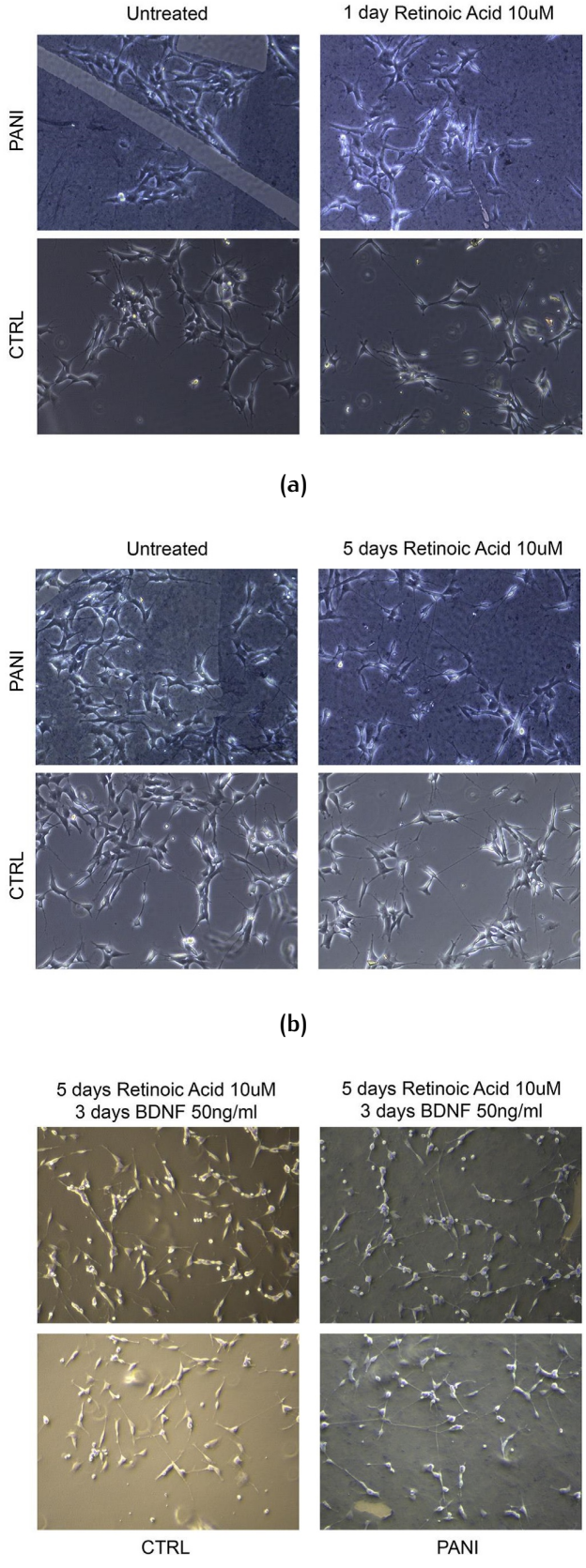

Figure 3.41: *Differentiation of SH-SY5Y cells: after 1 day (a), 5 days (b) of treatment with 10 μM retinoic acid and (c) after 5 days of treatment with 10 M retinoic acid and 3 days with BDNF 50 ng/ml on PANI and on microscope glass slides. Picture taken from [79]*

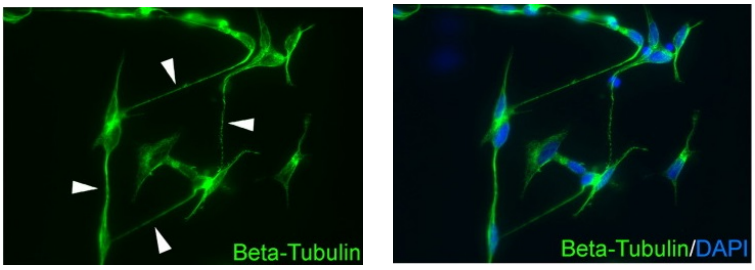

Figure 3.42: *SH-SY5Y cells differentiated on PANI. Immunocytochemistry for beta tubulin (green) and DAPI (blue) of SH-SY5Y cells. For immunofluorescence, an anti-beta tubulin primary antibody (1:500, Santa Cruz) and the Alexa Fluor 488-conjugated goat anti-mouse IgGs secondary antibody (1:500, Life Technologies) were used. Immunofluorescence analysis was performed using the Zeiss Observer Z.1 Microscope with a PlanApo oil immersion lens (20, NA 1.4)[79].*

following the guidelines of the French National Institute of Health and Medical Research (INSERM, protocol N007.08.01) and the Kazan Federal University on the use of laboratory animals (ethical approval by the Institutional Animal Care and Use Committee of Kazan State Medical University N9-2013). The animals were decapitated and the brain, once removed, was rapidly placed into oxygenated (95%O_2–5%CO_2) ice-cold (2–5°C) artificial cerebrospinal fluid (ACSF) of the following composition (in mM): 126 NaCl, 3.5 KCl, 2 CaCl2, 1.3 MgCl2, 25 NaHCO3, 1.2 NaH2PO4, and 11 glucose 11, pH 7.4. Slices of about 500 µm were cut using a Vibratome (VT 1000E; Leica) and kept in oxygenated ACSF at room temperature (20–22°C) before use.

Whole-cell recordings were performed using pipette solutions of the following composition (mM): 140 CsF, 1 CaCl2, 10 HEPES, 10 EGTA with pH 7.3. Recordings were acquired with Clampex 10.3 software and digitized (10kHz) on-line using a Digidata 1322 (Axon Instruments).

To successfully perform the final experiment it was necessary to study the final system (cell-memristor-cell) dividing it in two separate experiments (neuron-memristor and memristor-neuron) in order to verify the feasibility and to select the best approach for the result.

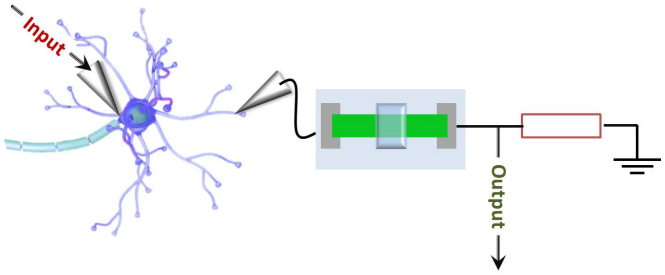

Figure 3.43: *Scheme of test: the output signal of the cell constitutes the input for the memristive device.*

First test: Could a neuron drive a memristor?

In the first test, in which the output of one neuron was addressed to one electrode of the memristor, we wanted to understand if the typical firing output of this kind of cells is functional for the memristive device and thus if its conductivity could be varied by this signal. The simplified scheme of the test is reported in Figure 3.43 while in Figure 3.44 a) is reported the neuronal cell involved in the experiment and in Figure 3.44 b) the typical activating pulse given to the cell(s) and the relative firing of the neuron. The excitations of the nervous cell provided by these pulses result in the generation of quite reproducible spikes that thus, can be applied to the memristor.

From Figure 3.43, once that the cells are stimulated by the activating pulse, they are going to produce an output signal (a voltage stimulus) that will feed the serial connection of the organic memristive device and a resistor. Clearly, the voltage drop in the circuit acquired just after the memristor is proportional to the memristance of the device.

We reported in the bottom part of the Figure 3.45 the nervous cell firing profile compared with the voltage drop acquired after the memristive device (top part of the graph). Even if the spikes provided by the cell are mostly reproducible, the memristive response seams to follow an increasing trend with the number of applied spikes. The shape of the peaks in both cases remains

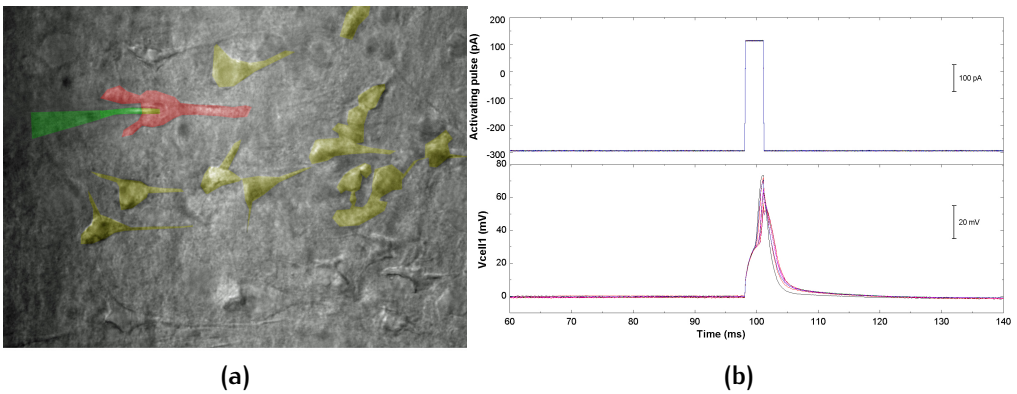

Figure 3.44: *Panel a): the neuronal cell involved in the experiment and the pipette of patch-clamp are respectively highlighted in red and in green; other cells are in yellow. Panel b) the activating pulse given to the cell(s) (top part) and the relative firing (bottom part).*

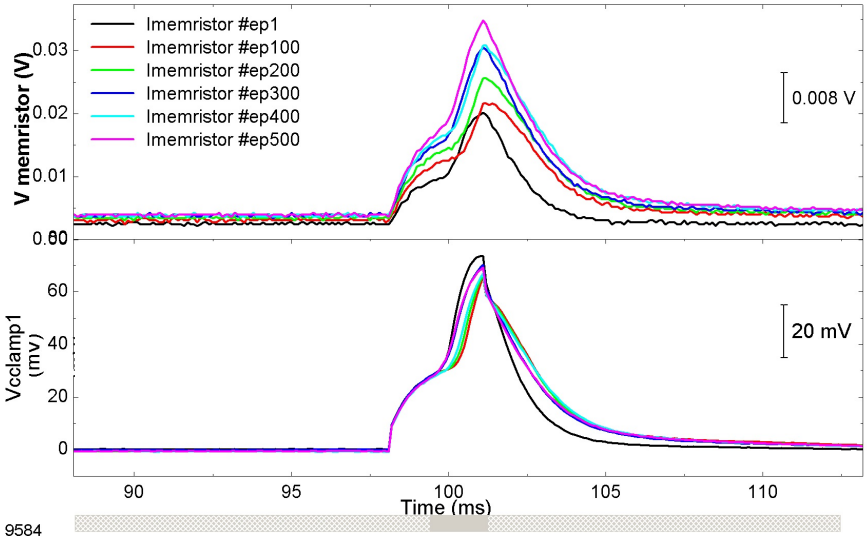

Figure 3.45: *Temporal dependences of the output of the neuronal cell (bottom) and of the memristive device (top) measured according to the scheme of Figure 3.43 in function of the number of the stimuli (reported in the legend).*

unchanged for all the experiment but the amplitude of the device output varies. Since the only input that feeds the memristor is the output of the cell, the increasing of the voltage drop after the device is due to the raising number of incoming stimuli that enhance the memristor conductivity of mostly 2 times.

The same trend can be better observed in Figure 3.46 where the temporal evolution of the output of the neuronal cell (in black) and of the memristive device (in red) are reported.

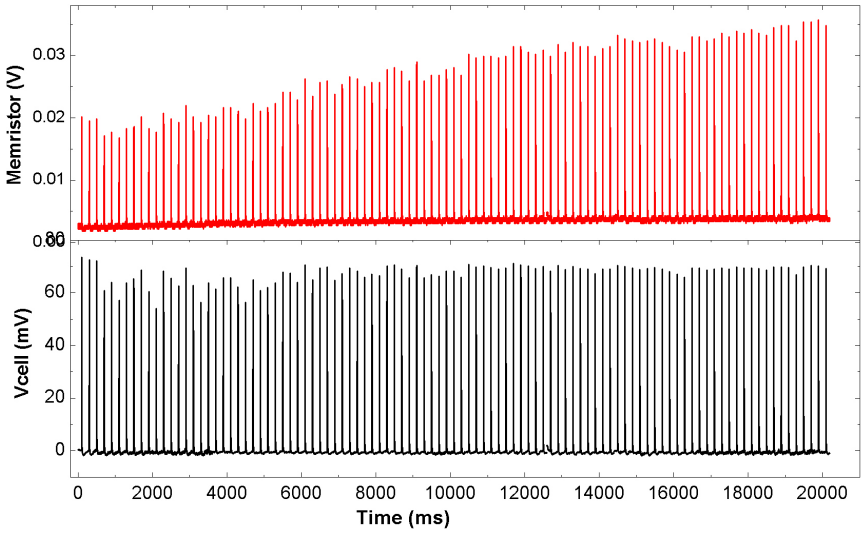

Figure 3.46: *Temporal evolution of the output of the neuronal cell (in black) and of the memristive device (in red) for the whole sequence of applied pulses measured according to the scheme of Figure 3.43*

Thus, in this first set of experiments we have demonstrated that the addressing of the spiking of the neuron cell to a memristive device increases its transmission function.This effect is the direct demonstration of the implementation of the synaptic temporal integration of the stimuli with an electrochemical device: high frequency of action potentials in the presynaptic neuron elicits postsynaptic potentials that overlap and summate with each other allowing the potential to reach the threshold to generate a following action potential [96, 85].

Second test: Could a memristor drive a neuron?

In the second experiment instead we wanted to face the opposite problem, aiming to demonstrate that the memristive output is a good input signal for the neuronal firing. So the memristor-resistor couple was powered by sequence of pulses from the external generator, analogues to the activation pulses, while the output was used for excitation of the nervous cell. The scheme and the results of this further test are reported in Figure 3.47, Figure 3.48 and Figure 3.49 respectively.

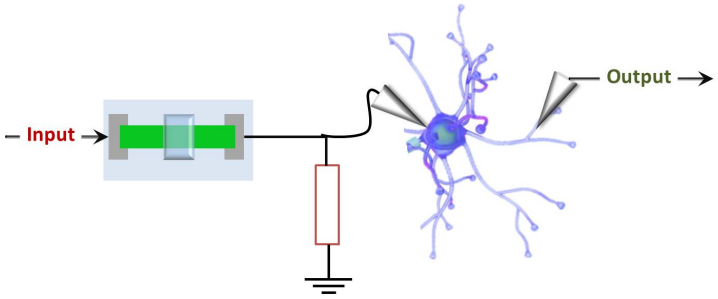

Figure 3.47: *Scheme of test: the output signal of the memristor is addressed to the neuronal cell.*

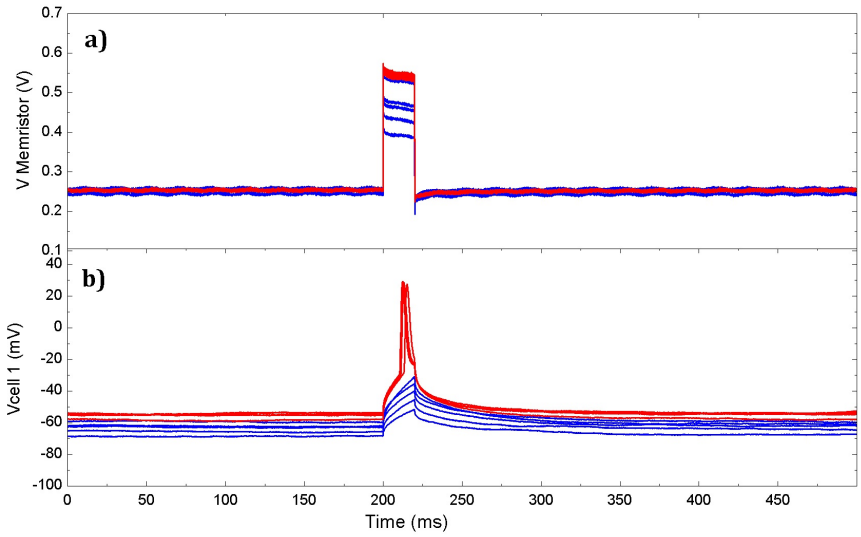

Figure 3.48: *Temporal dependences of the output of the neuronal cell (panel b)) and of the memristive device (panel a)) measured according to the scheme of Figure 3.47 in function of the number of the stimuli (stimuli from 1 to 130 are in blue, from 130th to the end are in red)*

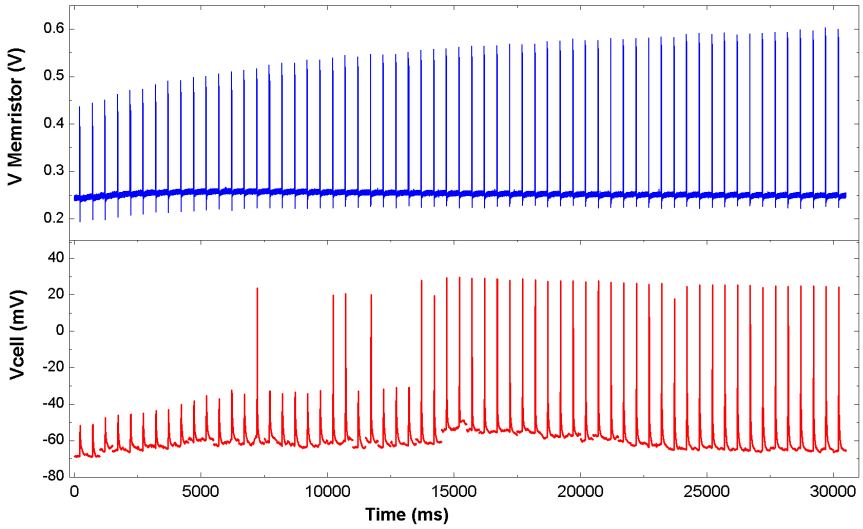

Figure 3.49: *Temporal evolution of the output of the neuronal cell (in red) and of the memristive device (in blue) for the whole sequence of applied pulses measured according to the scheme of Figure 3.47*

In Figure 3.48 a) the signal obtained from the memristor voltage drop follows the same increasing trend reported in the previous experiment but in this case the shape of this output has the profile of the pulses provided by the external generator, as expected. Moreover even in this second test, the memristor output has an increasing trend with the number of spikes that the generator provided (Figure 3.49). Initially, so for a low number of stimuli, the output of the device doesn't exceed the neuronal activation threshold and this results in failed firing of the cell (blue curves in Figure 3.48 a) and b)). The direct demonstration of this is the low amplitude and the shape of the blue curves in Figure 3.48 b) that are the result of the input stimulus mediated by the RC circuit of the set up.

However after that the number of spikes reached a threshold value, the memristive transmitted signal amplitude is enough for the cell activation and this results in the variation of the shape of the neuronal signal and a wider amplitude (red curves in Figure 3.48 a) and b)).

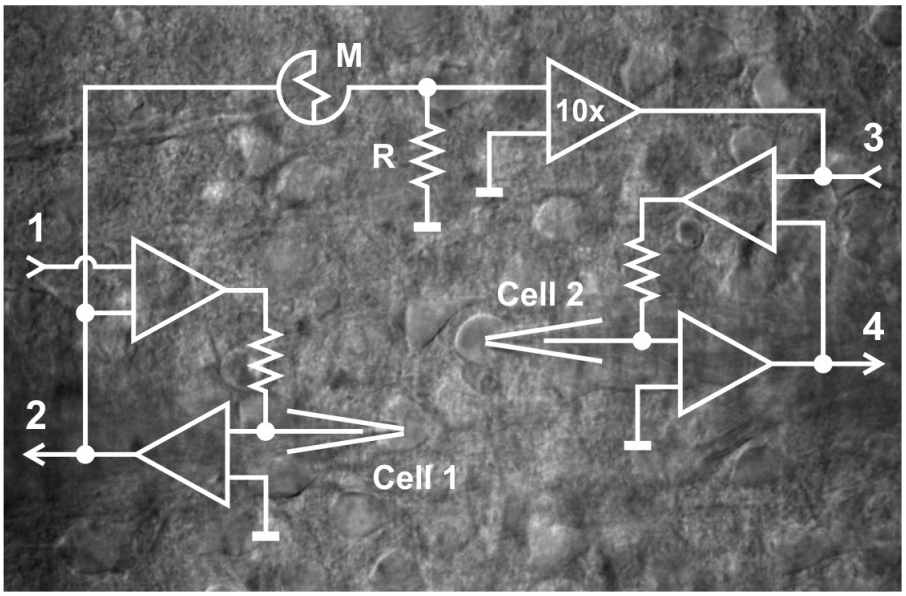

Figure 3.50: *Scheme of the third experiment: Cell 1 is loaded by pulses from the external generator; output signal goes to the serial connection of the memristor (M) and resistor (R); the signal from the central point of its serial circuit goes to the second cell.*

Final test: Could a memristor be an artificial synapse?

So finally in the third experiment, we involved two nervous cells bridged by a memristor. The first nervous cell is excited by the external pulses and its voltage output feeds the circuit formed by the electrochemical device and resistor. The memristive output is the input of the second nervous cell. The scheme of the hybrid circuit between cells and device is reported in Figure 3.50 where point 1 is the application of the activating pulse for the cell 1 and point 2,3 and 4 are the acquisition points of the circuit for the outputs coming from cell 1, memristor and cell 2, respectively. The signals resulting from these acquisitions are plotted in Figure 3.51.

From Figure 3.51, the stimulation of the first cell produces a reproducible output spiking (blue curve) that affects the voltage drop across the memristor that increases the value acquired of mostly 3 times (red curve). This, in analogy with the first test reported above, is due to the enhancement of the conductivity of the device that increasing the current that can flow through it, heightens the potential applied to the second cell. This latter one, until the incoming signal

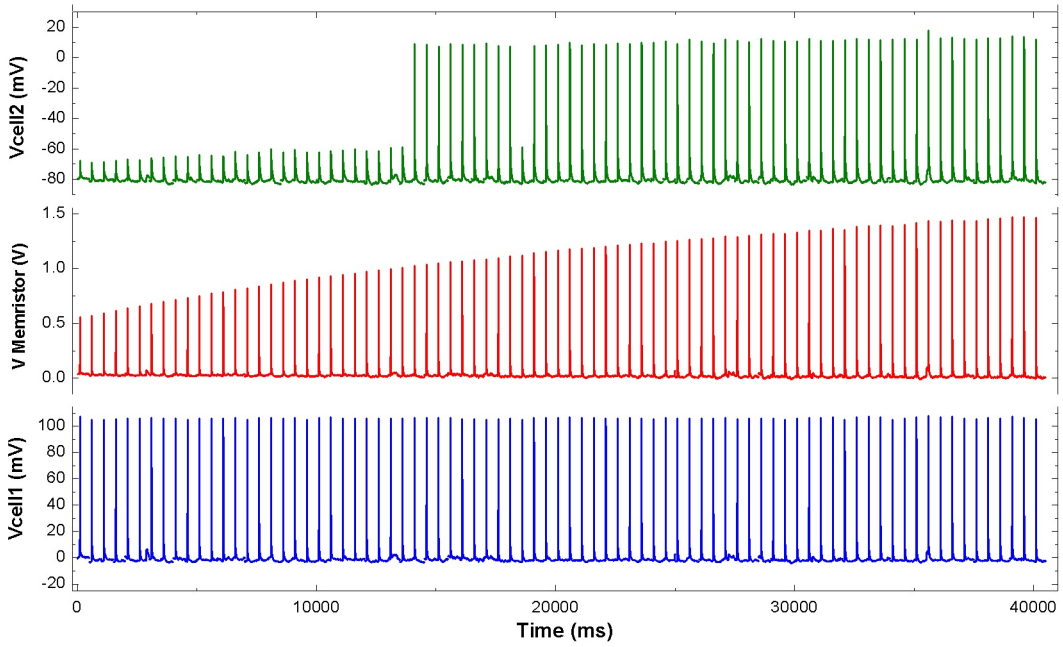

Figure 3.51: *Temporal evolution of the output of the first neuronal cell (in blu), of the memristive device (in red) and of the second neuron (in green) for the whole sequence of applied pulses measured according to the scheme of Figure 3.50.*

from the memristive device is not enough for its activation, doesn't produce any firing events and its voltage pulses slightly increase their amplitude following the memristor's increasing trend. When the received signal overcomes the activation threshold, the cell started to fire, in analogy with the second test already performed and the already mentioned synaptic temporal integration [96, 85].

What we can conclude is that after the two preliminary tests that successfully demonstrated the possibility of a bidirectional communication between neuronal cells and organic memristive devices, this third experiment demonstrated that the device used can be effectively considered as the first step towards the realization of a working "synapse prosthesis" able to learn and perform variation of the synaptic strength in accordance with the Hebb's rule and the already mentioned synaptic temporal integration.

4 CONCLUSIONS

The results of this thesis can be classified in two strongly interconnected ensembles: memristive neuromorphic applications, in which we reported the ability of such kind of device to mimicking synaptic neuromorphic functions, and the creation of functional bio-interfaces between memristors and neuronal cells, in which we described the possible creation of hybrid circuits made up from cells and device, in which the memristor plays the important role of artificial synapse.

In the field of the neuromorphic applications, our works contributed both in the mimicking of the homo-and heterosynaptic plasticity features demonstrating that a single organic memristor is able to implement correctly the LTP and LTD functions following the already walked street of the variation in the conductivity in function of the polarity and the frequency of the applied pulses. Moreover we decided to go beyond this result and implement with a fixed pulse the two neuromorphic functions varying just the frequency of the stimuli, thus mimicking exactly the biological behaviour. In the same direction we implemented the more complex heterosynaptic plasticity features varying the device standard geometry including a second PANI channel whose function is the modulation of the conductive properties of the other polyaniline layer. We initially demonstrated that the variation of the first channel voltage affects the other channel output current and furthermore that the result of this modulation is a gradual increasing of the conductivity of the second PANI layer.

Once demonstrated that a single memristive unit is able to implement classical neuromorphic functions, we moved on the realization of complex networks of memristors, that once again mimics the way in which a neuronal network "processes" incoming data. We successfully implemented the elementary perceptron and we trained it to perform linearly separable classification of the input combination of the NAND and NOR logic functions. Once again we went beyond this initial results and we realized an artificial neuronal network that performs linearly non separable tasks (XOR logic function) and that is to be considered a precursor of a double layer perceptron. The gap between our ANN and a double layer perceptron is the implementation of the backpropagation training method that we substituted with a simpler algorithm in order to face the device variability.

In the field of the bio-electronic, the contribution of this thesis is the providing evidences of the the possibility of establish a bidirectional communication between neuronal cells and organic memristive devices, demonstrating that on the one hand, neuronal cells firing outputs can increase the memristive conductivity and on the other hand, that stimuli provided by the electrochemical device can be correctly "processed" by the nervous cell that fires following the synaptic temporal integration mechanism. Moreover, we have provided evidences that a memristive device, whose synapse mimicking properties are well known, can bridge two nervous cells preserving their biological communication mechanisms. In other words, the organic memristive device can be effectively considered as the first step towards the realization of a working "synapse prosthesis" able to learn and perform variation of the synaptic strength in accordance with the Hebb's rule.

Moreover, the already mentioned results have been accompanied by the developing of a new and non-invasive method for the detection of the conductivity variation in organic memristive devices in which we took advantage of the intrinsic electrochromic feature of the conductive polymer to detect the conductivity switching of the device. Furthermore we also exploited the possibility of driving an organic memristive device as a transistor, thus varying the conductive properties of the device with the action of the modulating gate voltage. It came out the creation of an all-in-one hybrid device with the typical gate modulation of the electrochemical transistors and two internal memory states corresponding to the oxidated and reduced polymer forms.

A APPENDIX

Contents

A.1 LANGMUIR BLODGETT FILMS

Since 1917, the studies on the formation of a monolayer at an air-water interface and the deposition of such a film was carried by Langmuir and two of his collaborators Blodgett and Schaefer. In her first paper published in 1934, Katharine Blodgett describes the deposition technique that, using a glass substrate with a vertical dipping brought to the deposition of fatty acid multilayer films. Five years later, Vincent Schaefer invented the horizontal dipping deposition method in which the substrate "is hold face down in a nearly horizontal position and lowering it onto the surface of the water in a tray covered with a monolayer of urease" .

The typical configuration of the instrument for the analysis and the deposition of Langmuir films is reported in Figure A.1.

Most of the monolayer forming substances are molecules composed of a hydrophilic and a hydrophobic part, called amphiphiles or surface active agents (in short surfactants); in order to deposit them, they first need to be dissolved in a proper solvent, forming a stable solution that is going to be spread at the interface between air and a subphase. By definition a subphase is the liquid

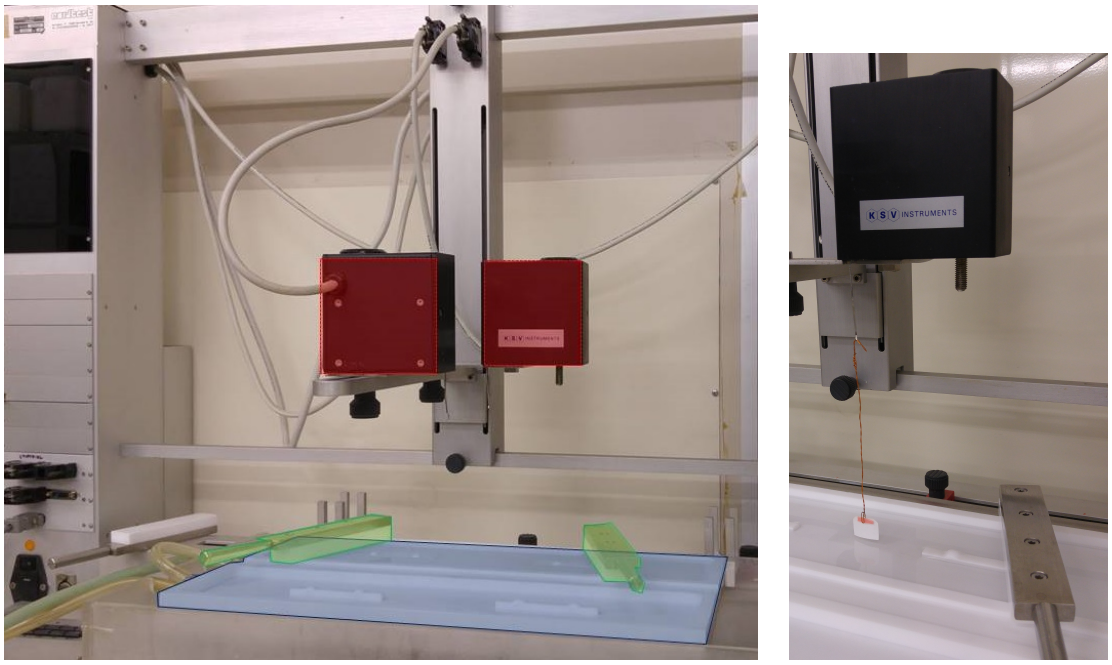

(a) . (b) .

Figure A.1: *KSV 5000 trough apparatus for analysis and the deposition of Langmuir films: in red the microbalances; in blu the trough (trough being the term commonly use to describe the water tank in which LB or LS experiment are performed); in green the moving barriers.*

on which the monolayer is going to be formed. Classically, the subphase is demineralized-deionized water with a 18.5 MΩ to ensure that the properties of the monolayer are not affected by the possible interactions between the surfactant polar head and minerals contained in natural water. Once that the solution in ready and stable, this must be spread on the water subphase and, in case of a volatile solvent, allow its evaporation before starting the compression of the molecules with two barriers to form the film. This step is necessary since once that the molecules are injected, they start to spread all over the available surface area forming a 2D gas state with relatively large distances between the molecules. Applying an external force to those floating molecules, a compression of them will induce a progressive ordered distribution and organization of the surfactants on the surface of the subphase passing from a disordered 2D gas state to a solid film. This process goes through several phase transitions that can therefore be identified simply by measuring the surface pression

(Π-a) an isotherm, in other words by determining the pressure versus area per molecule curve at constant temperature.

Since the surface pressure Π is defined as the difference between the surface tension of pure subphase (for example water) and the same subphase covered with molecules ($\Pi = \gamma_0 - \gamma$), a simple way to determine this physical parameter is the Wilhelmy plate (Figure A.1b).

In this method a plate, most often made of paper, is partially immersed in water subphase and the total force acting on it (F_0) is given by the sum of three forces: the gravity (F_G)and the surface tension (γ) both acting downwards and the buoyancy of the plate (F_B), acting upward. This F_0 is acquired at the begin of the measurement before the injecting of the surfactant solution.

$$F = F_G + \gamma \cos\Theta.P - F_B \tag{A.1}$$

where P is the perimeter of the plate and Θ is the contact angle of the liquid on the solid plate. So in the hypothesis of a completely wetted plate, the term $\cos\Theta = 1$ and the equation can be simplify:

$$F = F_G + \gamma.P - F_B \tag{A.2}$$

Since this force depend on the surface tension, once that the solution is spread on the subphase, the total force (F) undergoes a deep variation due to the modification of the γ. Measuring the dynamical change of force F in response of the variation of the distance between the molecules, is possible to estimate the surface pressure of the film comparing F and F_0 :

$$\Pi = \gamma_0 - \gamma = \frac{F_0 - F}{P} \tag{A.3}$$

So, during the compression of the molecules, pressure and area per molecule* are recorded until the value of the pressure reaches a pre-setted threshold value, in our experiment it was set to 10mN/m.

At the beginning, the area per molecule in the gas state is large and the pressure can be directly calculated from the ideal gas law applied in the case of a 2D gas:

$$PA = NkT \tag{A.4}$$

where P is the pressure of the 2D gas, A the total area of the container, N the number of molecules and kT the Boltzmann constant times the temperature.

Further reduction of the area between the molecules will induce initially the transition from a gas to a liquid phase, arranging the molecules in a coherently way but leaving them in a certain degree of disorder and then it will induce the transition from liquid to solid phase where the molecules are densely packed and the pressure reaches its maximum value. At this stage the order between the surfactant is perfect and any further compression will induce the collapse of the film, breaking the solid film and forming different structures such as bi- or trilayers and eventually forms a micro-crystallites. So the final pressure value at which the barriers must stop their run must be selected in order to combine two effects: do not exceed the maximum values for the film but in the same time guarantee a sufficient compression of the molecules; once reached this state, the film transfer, the deposition, must be archived in two ways (Figure A.2): a vertical deposition, developed by Blodgett and Langmuir and a horizontal lifting method, named as Langmuir-Schaefer (LS) method. This latter method is preferable in case of rigid film in which the crystalline order need to be preserved and consist in a slow approach of the substrate to the monolayer until the perfect total horizontal contact is reached; then the substrate is gently removed from the subphase and the residual water on the sample is removed, blowing compress air, to preserve the homogeneity of the monolayer.

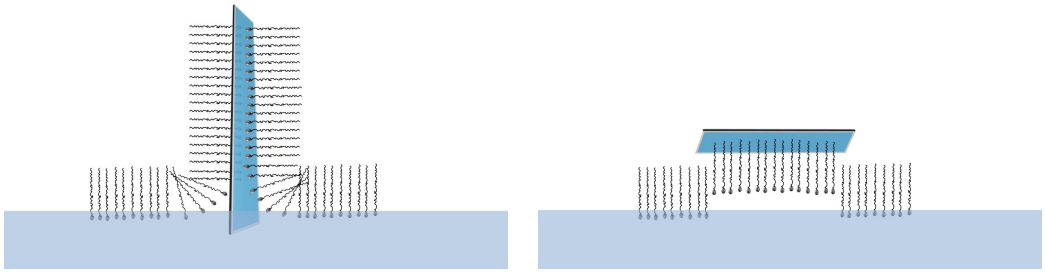

(a) *Langmuir-Blodgett.* **(b)** *Langmuir-Schaefer.*

Figure A.2: *Schematic representation of the vertical (Langmuir-Blodgett) and horizontal (Langmuir-Schaefer) multilayer films transfer method.*

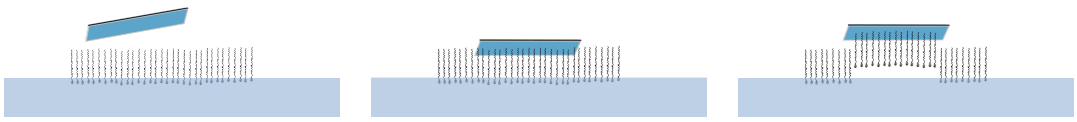

(a) . **(b)** . **(c)** .

Figure A.3: *Schematic representation of the horizontal (Langmuir-Schaefer) multilayer films transfer method.*

B ACKNOWLEDGEMENTS

I'd like to express my gratefulness to my Tutor Dr. Salvatore Iannotta for giving me the possibility of being involved in the MaDELeNA project and for the support he gave me during these 3 years. I have to reserve a special mention for all the people I had the pleasure to collaborate with starting from Parma's group composed by Dr. Baldi, Dr. Dimonte and Dr. Erokhina that embraced me and guided me from day 1 to the end. Sharing ideas, doubts, perspectives and long hours of experiments has been great and taught me more than expected.

Furthermore they gave me the chance of get in contact with other groups I enjoyed to work with such as Dr. Emelyanov, Dr. Lapkin and Dr. Demin from the National Research Centre Kurchatov Institute in Moscow and Dr Khazipov from Institut de Neurobiologie de la Mediterranee-Institut National de la Sante et de la Recherche Medicale in Marseille. Dedicated and enthusiast people make the work fascinating and easier... so thank you.

From MaDEleNA project I also want to thank Dr. Verucchi, Dr. Pederzoli and Dr. Pasquardini from Trento unit for their advices and suggestions and also Prof. George Malliaras that hosted me in his lab (Department of BioElectronics Centre Microelectronics of Provence, Gardanne, France) showing me his bright and smart vision of science.

The most special thanks must be reserved to Dr. Erokhin that with the daily confrontation and with his curiosity, motivated and stimulated me. The exemplary dedication, passion and enthusiasm he put in his job were a priceless guide to form me as a "tiny researcher".

Finally, I cannot conclude my Acknowledgements without mentioning the wonderful family I have....Mom, Daddy and Stefano, you supported me in every decision i made and in every moment I felt your unconditional love following me, despite the distance. And finally Serena who patiently (a lot of patience!) has been for years the companion of many adventures, a safe heaven where to came back every evening....

BIBLIOGRAPHY

[1] Stanford University. Stanford Electronics Laboratories et al. *Adaptive "adaline" neuron using chemical "memistors."*. 1960. URL: https://books.google.it/books?id=Yc4EAAAAIAAJ (cit. on p. 1).

[2] R.M. Fano. *Electromagnetic Fields, Energy, and Forces*. M.I.T. core curriculum program in electrical engineering series. Wiley, 1960. URL: https://books.google.it/books?id=RCBRAAAAMAAJ (cit. on p. 2).

[3] L.O. Chua. "Memristor-The missing circuit element". In: *Circuit Theory, IEEE Transactions on* 18.5 (1971), pp. 507–519. ISSN: 0018-9324. DOI: 10.1109/TCT.1971.1083337 (cit. on pp. 2, 3).

[4] Strukov; Snider; Stewart; Williams. "The missing memristor found". In: *Nature* 453 (2008), pp. 80–83. ISSN: 0028-0836. DOI: 10.1038/nature06932 (cit. on pp. 2, 5).

[5] L. O. Chua and Sung Mo Kang. "Memristive devices and systems". In: *Proceedings of the IEEE* 64.2 (1976), pp. 209–223. ISSN: 0018-9219. DOI: 10.1109/PROC.1976.10092 (cit. on pp. 3, 4, 16).

[6] F. Corinto, P. P. Civalleri, and L. O. Chua. "A Theoretical Approach to Memristor Devices". In: *IEEE Journal on Emerging and Selected Topics in Circuits and Systems* 5.2 (2015), pp. 123–132. DOI: 10.1109/JETCAS.2015.2426494 (cit. on p. 4).

[7] Williams. "How we found the missing memristor". In: *IEEE SPECTRUM* (2008) (cit. on p. 5).

[8] Victor Erokhin, Tatiana Berzina, and Marco P Fontana. "Hybrid electronic device based on polyaniline-polyethyleneoxide junction". In: *Journal of applied physics* 97.6 (2005), p. 064501 (cit. on pp. 6, 9, 25, 31).

[9] Rainer Waser and Masakazu Aono. "Nanoionics-based resistive switching memories". In: *Nature materials* 6.11 (2007), pp. 833–840 (cit. on p. 6).

[10] Terje A Skotheim. *Handbook of conducting polymers*. CRC press, 1997 (cit. on p. 7).

[11] DM De Leeuw et al. "Stability of n-type doped conducting polymers and consequences for polymeric microelectronic devices". In: *Synthetic Metals* 87.1 (1997), pp. 53–59 (cit. on p. 7).

[12] Liming Dai. *Intelligent macromolecules for smart devices: from materials synthesis to device applications*. Springer Science & Business Media, 2004 (cit. on pp. 7, 8).

[13] Richard Balint, Nigel J Cassidy, and Sarah H Cartmell. "Conductive polymers: towards a smart biomaterial for tissue engineering". In: *Acta biomaterialia* 10.6 (2014), pp. 2341–2353 (cit. on pp. 7, 8).

[14] Kenji Hyodo. "Electrochromism of conducting polymers". In: *Electrochimica acta* 39.2 (1994), pp. 265–272 (cit. on p. 8).

[15] Tetsuhiko Kobayashi, Hiroshi Yoneyama, and Hideo Tamura. "Electrochemical reactions concerned with electrochromism of polyaniline film-coated electrodes". In: *Journal of electroanalytical chemistry and interfacial electrochemistry* 177.1 (1984), pp. 281–291 (cit. on p. 9).

[16] M.A. Shishov I.Yu. Sapurina. 2012-09-12. DOI: 10.5772/48758 (cit. on p. 9).

[17] Tatiana Berzina, Victor Erokhin, and MP Fontana. "Spectroscopic investigation of an electrochemically controlled conducting polymer-solid electrolyte junction". In: *Journal of applied physics* 101.2 (2007), p. 024501 (cit. on pp. 9, 31).

[18] Tatiana Berzina et al. "Electrochemical Control of the Conductivity in an Organic Memristor: A Time-Resolved X-ray Fluorescence Study of Ionic Drift as a Function of the Applied Voltage". In: *ACS Applied Materials & Interfaces* 1.10 (2009), pp. 2115–2118. DOI: 10.1021/am900464k (cit. on pp. 9, 31).

[19] Tatiana Berzina et al. "Optimization of an organic memristor as an adaptive memory element". In: *Journal of Applied Physics* 105.12 (2009), p. 124515 (cit. on p. 10).

[20] Konstantin Gorshkov et al. "Organic memristor based on the composite materials: Conducting and ionic polymers, gold nanoparticles and graphenes". In: *Procedia Computer Science* 7 (2011), pp. 248–249 (cit. on p. 10).

[21] TS Berzina et al. "Investigation of electrical properties of organic memristors based on thin polyaniline-graphene films". In: *Russian Microelectronics* 42.1 (2013), pp. 27–32 (cit. on p. 10).

[22] Tatiana Berzina et al. "Role of the solid electrolyte composition on the performance of a polymeric memristor". In: *Materials Science and Engineering: C* 30.3 (2010), pp. 407–411 (cit. on p. 10).

[23] Valentina Allodi, Victor Erokhin, and MP Fontana. "Effect of temperature on the electrical properties of an organic memristive device". In: *Journal of Applied Physics* 108.7 (2010), p. 074510 (cit. on p. 10).

[24] Victor Erokhin et al. "Non-equilibrium electrical behaviour of polymeric electrochemical junctions". In: *Journal of Physics: Condensed Matter* 19.20 (2007), p. 205111. URL: http://stacks.iop.org/0953-8984/19/i=20/a=205111 (cit. on p. 10).

[25] VV Erokhin, TS Berzina, and MP Fontana. "Polymeric elements for adaptive networks". In: *Crystallography Reports* 52.1 (2007), pp. 159–166 (cit. on p. 11).

[26] Anteo Smerieri et al. "Polymeric electrochemical element for adaptive networks: Pulse mode". In: *Journal of Applied Physics* 104.11 (2008), p. 114513 (cit. on p. 11).

[27] Anteo Smerieri et al. "A functional polymeric material based on hybrid electrochemically controlled junctions". In: *Materials Science and Engineering: C* 28.1 (2008), pp. 18–22 (cit. on p. 11).

[28] Silvia Battistoni, Alice Dimonte, and Victor Erokhin. "Organic Memristor Based Elements for Bio-inspired Computing". In: *Advances in Unconventional Computing*. Springer, 2017, pp. 469–496 (cit. on p. 12).

[29] X. Zhang et al. "A Physarum-Inspired Approach to Optimal Supply Chain Network Design at Minimum Total Cost with Demand Satisfaction". In: *ArXiv e-prints* (2014). arXiv: 1403.5345 (cit. on p. 12).

[30] J. G. Holland Whiting, B. de Lacy Costello, and A. Adamatzky. "Sensory fusion in Physarum polycephalum and implementing multi-sensory functional computation". In: *ArXiv e-prints* (2014). arXiv: 1403.4795 (cit. on p. 12).

[31] Sung Hyun Jo et al. "Nanoscale memristor device as synapse in neuromorphic systems". In: *Nano letters* 10.4 (2010), pp. 1297–1301 (cit. on pp. 12, 16, 17).

[32] C.S. Foster M.; Sherrington. *Textbook of Physiology, volume 3 (7th ed.)* Macmillan., 1897 (cit. on p. 12).

[33] D. Purves et al. *Neuroscience*. Sinauer Associates, 2001. ISBN: 9780878937431. URL: https://books.google.ca/books?id=F4pTPwAACAAJ (cit. on pp. 12–15, 53).

[34] John R. Hughes. "Post-Tetanic Potentiation". In: *Physiological Reviews* 38.1 (1958), pp. 91–113. eprint: http://physrev.physiology.org/content/38/1/91.full.pdf. URL: http://physrev.physiology.org/content/38/1/91 (cit. on p. 13).

[35] Donald Olding Hebb. *The organization of behavior: A neuropsychological theory*. Psychology Press, 2005 (cit. on pp. 14, 16).

[36] Craig H Bailey et al. "Is heterosynaptic modulation essential for stabilizing hebbian plasiticity and memory". In: *Nature Reviews Neuroscience* 1.1 (2000), pp. 11–20 (cit. on p. 14).

[37] Tim VP Bliss, Graham L Collingridge, et al. "A synaptic model of memory: long-term potentiation in the hippocampus". In: *Nature* 361.6407 (1993), pp. 31–39 (cit. on p. 14).

[38] Robert C. Malenka, Nicoll, and Roger A. "Long-Term Potentiation–A Decade of Progress?" In: *Science* 285.5435 (1999), pp. 1870–1874. ISSN: 0036-8075. DOI: 10.1126/science.285.5435.1870 (cit. on p. 14).

[39] Marina Chistiakova et al. "Homeostatic role of heterosynaptic plasticity: models and experiments". In: *Frontiers in computational neuroscience* 9 (2015) (cit. on p. 14).

[40] Arun V Holden and William Winlow. *The Neurobiology of Pain: Symposium of the Northern Neurobiology Group, Held at Leeds on 18 April, 1983*. Manchester University Press, 1984 (cit. on p. 15).

[41] You Zhou and Shriram Ramanathan. "Mott Memory and Neuromorphic Devices". In: *Proceedings of the IEEE* 103.8 (2015), pp. 1289 –1310 (cit. on p. 16).

[42] Saptarshi Mandal et al. "Novel synaptic memory device for neuromorphic computing". In: *Scientific reports* 4 (2014) (cit. on p. 16).

[43] Sylvain Saïghi et al. “Plasticity in memristive devices for spiking neural networks”. In: *Frontiers in neuroscience* 9 (2015), p. 51 (cit. on pp. 16, 17).

[44] Gregory S Snider. “Self-organized computation with unreliable, memristive nanodevices”. In: *Nanotechnology* 18.36 (2007), p. 365202 (cit. on p. 16).

[45] Greg S Snider. “Spike-timing-dependent learning in memristive nanodevices”. In: *2008 IEEE International Symposium on Nanoscale Architectures*. IEEE. 2008, pp. 85–92 (cit. on p. 16).

[46] Guo-qiang Bi and Mu-ming Poo. “Synaptic modification by correlated activity: Hebb’s postulate revisited”. In: *Annual review of neuroscience* 24.1 (2001), pp. 139–166 (cit. on p. 16).

[47] Joshua M Young et al. “Cortical reorganization consistent with spike timing–but not correlation-dependent plasticity”. In: *Nature neuroscience* 10.7 (2007), pp. 887–895 (cit. on p. 16).

[48] Guo-qiang Bi and Mu-ming Poo. “Synaptic modifications in cultured hippocampal neurons: dependence on spike timing, synaptic strength, and postsynaptic cell type”. In: *The Journal of neuroscience* 18.24 (1998), pp. 10464–10472 (cit. on p. 16).

[49] Hyongsuk Kim et al. “Memristor bridge synapses”. In: *Proceedings of the IEEE* 100.6 (2012), pp. 2061–2070 (cit. on p. 17).

[50] Shyam Prasad Adhikari et al. “Memristor bridge synapse-based neural network and its learning”. In: *IEEE Transactions on Neural Networks and Learning Systems* 23.9 (2012), pp. 1426–1435 (cit. on p. 17).

[51] Sergey E. Savel’ev Hao Jiang Rivu Midya Peng Lin-Miao Hu Ning Ge John Paul Strachan Zhiyong Li Qing Wu Mark Barnell Geng-Lin Li Huolin L. Xin R. Stanley Williams Qiangfei Xia J. Joshua Yang Zhongrui Wang Saumil Joshi. “Memristors with diffusive dynamics as synaptic emulators for neuromorphic computing”. In: *Nature materials* (2016) (cit. on p. 17).

[52] Omid Kavehei et al. “Memristor-based synaptic networks and logical operations using in-situ computing”. In: *Intelligent Sensors, Sensor Networks and Information Processing (ISSNIP), 2011 Seventh International Conference on*. IEEE. 2011, pp. 137–142 (cit. on p. 17).

[53] SG Hu et al. “Synaptic long-term potentiation realized in Pavlov’s dog model based on a NiOx-based memristor”. In: *Journal of Applied Physics* 116.21 (2014), p. 214502 (cit. on p. 17).

[54] Takeo Ohno et al. “Short-term plasticity and long-term potentiation mimicked in single inorganic synapses”. In: *Nature materials* 10.8 (2011), pp. 591–595 (cit. on pp. 17, 48, 50, 53).

[55] Ting Chang, Sung-Hyun Jo, and Wei Lu. “Short-term memory to long-term memory transition in a nanoscale memristor”. In: *ACS nano* 5.9 (2011), pp. 7669–7676 (cit. on pp. 17, 18).

[56] Wei He et al. “Enabling an integrated rate-temporal learning scheme on memristor”. In: *Scientific reports* 4 (2014) (cit. on pp. 17, 53).

[57] Matthew D Pickett, Gilberto Medeiros-Ribeiro, and R Stanley Williams. “A scalable neuristor built with Mott memristors”. In: *Nature materials* 12.2 (2013), pp. 114–117 (cit. on p. 18).

[58] C. H. Bennett et al. “Supervised learning with organic memristor devices and prospects for neural crossbar arrays”. In: *Proceedings of the 2015 IEEE/ACM International Symposium on Nanoscale Architectures (NANOARCH¿¿15)*. 2015, pp. 181–186. DOI: 10.1109/NANOARCH.2015.7180609 (cit. on p. 18).

[59] Yuchao Yang, Bing Chen, and Wei D Lu. “Memristive Physically Evolving Networks Enabling the Emulation of Heterosynaptic Plasticity”. In: *Advanced Materials* 27.47 (2015), pp. 7720–7727 (cit. on pp. 18, 59).

[60] F. Rosenblatt. *The Perceptron, a Perceiving and Recognizing Automaton Project Para*. Report: Cornell Aeronautical Laboratory. Cornell Aeronautical Laboratory, 1957. URL: https://books.google.cz/books?id=P_XGPgAACAAJ (cit. on p. 20).

[61] Frank Rosenblatt. "The perceptron: a probabilistic model for information storage and organization in the brain." In: *Psychological review* 65.6 (1958), p. 386 (cit. on p. 20).

[62] Frank Rosenblatt. *Principles of neurodynamics. perceptrons and the theory of brain mechanisms*. Tech. rep. DTIC Document, 1961 (cit. on p. 22).

[63] John J Hopfield. "Neural networks and physical systems with emergent collective computational abilities". In: *Proceedings of the national academy of sciences* 79.8 (1982), pp. 2554–2558 (cit. on p. 22).

[64] Xenofon Strakosas, Manuelle Bongo, and Róisín M. Owens. "The organic electrochemical transistor for biological applications". In: *Journal of Applied Polymer Science* 132.15 (2015). ISSN: 1097-4628. DOI: 10.1002/app.41735 (cit. on p. 22).

[65] Peng Lin, Feng Yan, and Helen LW Chan. "Ion-sensitive properties of organic electrochemical transistors". In: *ACS applied materials & interfaces* 2.6 (2010), pp. 1637–1641 (cit. on p. 22).

[66] Zekra Mousavi et al. "Ion-Selective Organic Electrochemical Junction Transistors Based on Poly(3,4-ethylenedioxythiophene) Doped with Poly(styrene sulfonate)". In: *Electroanalysis* 21.3-5 (2009), pp. 472–479. DOI: 10.1002/elan.200804427 (cit. on p. 22).

[67] Peng Lin and Feng Yan. "Organic Thin-Film Transistors for Chemical and Biological Sensing". In: *Advanced materials* 24.1 (2012), pp. 34–51 (cit. on p. 22).

[68] Victor Erokhin and Marco P Fontana. "Electrochemically controlled polymeric device: a memristor (and more) found two years ago". In: *arXiv preprint arXiv:0807.0333* (2008) (cit. on p. 25).

[69] Fabien Alibart et al. "A Memristive Nanoparticle/Organic Hybrid Synapstor for Neuroinspired Computing". In: *Advanced Functional Materials* 22.3 (2012), pp. 609–616. ISSN: 1616-3028. DOI: 10.1002/adfm.201101935. URL: http://dx.doi.org/10.1002/adfm.201101935 (cit. on p. 25).

[70] X. Yan Y. Wang and R. Dong. "Organic memristive devices based on silver nanoparticles and DNA". In: *Organic Electronics* 15 (2014), pp. 3476–3481 (cit. on p. 25).

[71] Bernard Widrow, WH Pierce, and JB Angell. "Birth, life, and death in microelectronic systems". In: *Military Electronics, IRE Transactions on* 1051.3 (1961), pp. 191–201 (cit. on p. 25).

[72] Valentino Braitenberg. *Vehicles: Experiments in synthetic psychology*. MIT press, 1986 (cit. on p. 25).

[73] A. Ulman. *An Introduction to Ultrathin Organic Films: From Langmuir–Blodgett to Self–Assembly*. Elsevier Science, 2013. ISBN: 9780080926315. URL: https://books.google.it/books?id=4qb8BAAAQBAJ (cit. on p. 26).

[74] G Baldi et al. "Logic with memory: and gates made of organic and inorganic memristive devices". In: *Semiconductor Science and Technology* 29.10 (2014), pp. 104009–104014 (cit. on pp. 26, 28, 29, 42, 48, 74).

[75] Victor Erokhin. "Organic memristors: basic principles". In: *Proceedings of 2010 IEEE International Symposium on Circuits and Systems*. 2010 (cit. on pp. 27, 44, 53).

[76] Walter W. Focke, Gary E. Wnek, and Yen. Wei. "Influence of oxidation state, pH, and counterion on the conductivity of polyaniline". In: *The*

Journal of Physical Chemistry 91.22 (1987), pp. 5813–5818. DOI: 10.1021/j100306a059 (cit. on pp. 28, 29).

[77] N Gospodinova, P Mokreva, and L Terlemezyan. "Alternative concept of the transition emeraldine base-emeraldine salt". In: *Polymer* 34.6 (1993), pp. 1330–1332 (cit. on pp. 28, 29).

[78] Gianni Antonioli et al. "Spectrophotometric scanner for imaging of paintings and other works of art". In: *Conference on Colour in Graphics, Imaging, and Vision*. Vol. 2004. 1. Society for Imaging Science and Technology. 2004, pp. 219–224 (cit. on pp. 33, 38).

[79] Leon J Juarez-Hernandez et al. "Bio-hybrid interfaces to study neuromorphic functionalities: New multidisciplinary evidences of cell viability on poly (anyline)(PANI), a semiconductor polymer with memristive properties". In: *Biophysical chemistry* 208 (2016), pp. 40–47 (cit. on pp. 34, 75–80).

[80] ET Kang, KG Neoh, and KL Tan. "Polyaniline: a polymer with many interesting intrinsic redox states". In: *Progress in Polymer Science* 23.2 (1998), pp. 277–324 (cit. on p. 36).

[81] Victor Erokhin and MP Fontana. "Thin film electrochemical memristive systems for bio-inspired computation". In: *Journal of Computational and Theoretical Nanoscience* 8.3 (2011), pp. 313–330 (cit. on p. 36).

[82] S. Battistoni, A. Dimonte, and V. Erokhin. "Spectrophotometric characterization of organic memristive devices". In: *Organic Electronics* 38 (2016), pp. 79 –83. ISSN: 1566-1199. DOI: http://dx.doi.org/10.1016/j.orgel.2016.08.004 (cit. on pp. 37–41).

[83] Silvia Battistoni, Regina Burganova, and Victor Erokhin. "Organic memristive device as transistor: working principle and possible applications". In: *2016 IEEE Symposium Series on Computational Intelligence*. IEEE. 2016 (cit. on pp. 42, 43, 45–47).

[84] Giuseppe Tarabella et al. "Irreversible evolution of eumelanin redox states detected by an organic electrochemical transistor: en route to bioelectronics and biosensing". In: *Journal of Materials Chemistry B* 1.31 (2013), pp. 3843–3849 (cit. on p. 43).

[85] Paschalis Gkoupidenis et al. "Synaptic plasticity functions in an organic electrochemical transistor". In: *Applied Physics Letters* 107.26, 263302 (2015). DOI: http://dx.doi.org/10.1063/1.4938553. URL: http://scitation.aip.org/content/aip/journal/apl/107/26/10.1063/1.4938553;jsessionid=At92bF9wZtJWuQVHHhrsZAni.x-aip-live-06 (cit. on pp. 48, 50, 53, 83, 88).

[86] Richard M Shiffrin and Richard C Atkinson. "Storage and retrieval processes in long-term memory." In: *Psychological Review* 76.2 (1969), p. 179 (cit. on p. 50).

[87] James L McGaugh. "Memory–a century of consolidation". In: *Science* 287.5451 (2000), pp. 248–251 (cit. on p. 50).

[88] S. Battistoni, V.V. Erokhin, and S. Iannotta. "Simple circuit for heterosynaptic plasticity". In: *Advance functional material* (). in preparation (cit. on pp. 57, 58, 60, 61).

[89] V.A. Demin et al. "Hardware elementary perceptron based on polyaniline memristive devices". In: *Organic Electronics* 25 (2015), pp. 16 –20. DOI: http://dx.doi.org/10.1016/j.orgel.2015.06.015 (cit. on pp. 62, 64–67).

[90] A. V. Emelyanov et al. "First steps towards the realization of a double layer perceptron based on organic memristive devices". In: *AIP Advances* 6.11, 111301 (2016). DOI: http://dx.doi.org/10.1063/1.4966257 (cit. on pp. 68–70, 72, 74).

[91] Paul John Werbos. *The roots of backpropagation: from ordered derivatives to neural networks and political forecasting*. Vol. 1. John Wiley & Sons, 1994 (cit. on p. 72).

[92] Sebastian Golczak et al. "Comparative {XPS} surface study of polyaniline thin films". In: *Solid State Ionics* 179.39 (2008), pp. 2234 –2239. DOI: http://dx.doi.org/10.1016/j.ssi.2008.08.004 (cit. on p. 75).

[93] Silvia Battistoni, Alice Dimonte, and Victor Erokhin. "Organic Memristor Based Elements for Bio-inspired Computing". In: *Advances in Unconventional Computing: Volume 2: Prototypes, Models and Algorithms*. Ed. by Andrew Adamatzky. Cham: Springer International Publishing, 2017, pp. 469–496. ISBN: 978-3-319-33921-4. DOI: 10.1007/978-3-319-33921-4_18 (cit. on pp. 76, 77).

[94] Alice Dimonte, Silvia Battistoni, and Victor Erokhin. "Physarum in Hybrid Electronic Devices". In: *Advances in Physarum Machines: Sensing and Computing with Slime Mould*. Ed. by Andrew Adamatzky. Cham: Springer International Publishing, 2016, pp. 91–107. ISBN: 978-3-319-26662-6. DOI: 10.1007/978-3-319-26662-6_5 (cit. on p. 76).

[95] M Minlebaev et al. "Dynamic changes from depolarizing to hyperpolarizing GABAergic actions during giant depolarizing potentials in the neonatal rat hippocampus". In: (2015) (cit. on p. 78).

[96] Sarah J Etherington et al. "Synaptic Integration". In: *eLS*. John Wiley Sons, Ltd, 2001. ISBN: 9780470015902. DOI: 10.1002/9780470015902.a0000208.pub2. URL: http://dx.doi.org/10.1002/9780470015902.a0000208.pub2 (cit. on pp. 83, 88).